II. Overview of the Long Baseline Experiment

A. Prefatory Remark

The experiment is aimed at producing a conclusive result—positive or negative—concerning the neutrino oscillation signal suggested by the atmospheric neutrino results shown in Fig. I.3. We have designed it to be capable of reaching well below the lowest allowed values of Δm^2 and $\sin^2 2\theta$ in Fig. I.3 with high statistical precision and tight control of possible systematic errors. But we have also considered the dispersed distribution of the detectors in our design as a means to explore the relatively large allowed regions in Fig. I.3 in continuous steps of increasing sensitivity. These steps coincide well with reasonable expectations of the rates at which detectors can be built and funds are likely to flow to a long baseline neutrino oscillation experiment.

This experiment was proposed in 1992 and approved by the BNL-HENPAC as AGS Experiment 889 in 1993. In Fall 1994 the design was reviewed and validated by an external committee chaired by S. Aronson.

B. General nature of the experiment

The experiment makes use of the BNL AGS, which has the advantages of high proton intensity, fast, fine-time structured extraction of the external proton beam, and relatively low neutrino energy. All of these properties are vital for a successful neutrino oscillation experiment. High intensity allows a baseline as long as 68 km to be used effectively. Fast, time structured extraction of the proton beam allows the massive far detectors to be operated on the earth's surface by means of timing and live veto suppression of cosmic rays traversing the detectors. Low neutrino energy not only makes possible values of the quantity L/E_ν competitive with those at any proton accelerator in the world, but also limits the fraction of deep inelastically produced background events in the detector relative to the dominant quasielastic signal events.

An AGS based search for ν_μ oscillations can easily cover all of the region of $\Delta m^2 - \sin^2 2\theta$ indicated by the atmospheric neutrino data in Fig. I.3. These data specify the distance L at which the far detector should be located for a given average AGS produced neutrino energy, according to the oscillation probability equation, $P(\nu_\mu \leftrightarrow \nu_x) = \sin^2 2\theta_{\mu x} \sin^2(1.27\Delta m^2_{\mu x} L/E_\nu)$, where $\sin^2 2\theta_{\mu x}$ is the strength of mixing between ν_μ and ν_x, $\Delta m^2_{\mu x} \cong |m(\nu_\mu)^2 - m(\nu_x)^2|$ in eV^2, L is the neutrino source to detector distance in km, and E_ν is the neutrino energy in

GeV. A ratio $L/ < E_\nu > \cong 100$ is feasible in an AGS based experiment. It has the advantage over atmospheric neutrino experiments that the ν_e content in the produced ν_μ beam at the AGS is approximately 10^{-2}, which allows a sensitive search in the oscillation channel $\nu_\mu \leftrightarrow \nu_e$ to be made in addition to a high sensitivity search in the ν_μ disappearance mode. Although the ν beam energy of the AGS is below the effective threshold energy for τ production, depletion of the ν_μ in the beam at the far detector not attended by a corresponding large fractional change in the number of ν_e-induced events in that detector would provide *prima facie* evidence for oscillations in the channel $\nu_\mu \leftrightarrow \nu_\tau$. Furthermore, neutrino-induced single π^0 production through the flavor independent weak neutral current in each of the detectors of the AGS experiment provides direct normalization of the observed weak charged current event rates internal to each detector. This also makes possible a search for oscillations in the channel $\nu_\mu \rightarrow \nu_{(sterile)}$, and independent confirmation of any positive signal.

The apparatus will ultimately consist of four linearly aligned, widely separated, identical, massive imaging Cherenkov detectors 18 m in diameter $\times$ 18 m high at distances of approximately 1, 3, 24 and 68km from the neutrino source. The two closest detectors would be on the BNL site. The arrangement is shown schematically in Fig. 1. The count rates from the quasielastic reaction $\nu_\mu n \rightarrow \mu^- p$ in the upstream detectors, D1 and D3 —the dominant reaction in all four detectors—serve to disentangle the neutrino beam shape and intensity from the detector response, and to predict precisely and redundantly the count rates in the detectors D24 and D68. With the two far detector sites, the oscillation parameters, Δm^2 and $\sin^2 2\theta$, are overdetermined. If neutrino oscillations occur and result in a decrease of ν_μ–induced events in the detector, D24, by as little as a few percent, and proportionally more in the far detector, D68, Δm^2 and $\sin^2 2\theta$, will be specified with 1σ errors less than 15%, as shown in Fig. 34 in Chapter V.

Furthermore, as mentioned above, there is an independent method of normalization internal to each of the detectors. With the neutrino beam discussed below, approximately 20% of all ν_μ–induced events involve the weak neutral current (WNC) reactions $\nu n \rightarrow \nu n \pi^0$ and $\nu p \rightarrow \nu p \pi^0$, which occur with equal probability for all flavors of neutrinos. Consequently, the ratio of $\nu_\mu n \rightarrow \mu^- p$ events to the WNC (π^0) events in each detector will serve as an additional means of normalization and redundant identification of a positive neutrino oscillation signal. A detailed discussion of the measurement of WNC (π^0) is given below, along with WCC and WNC backgrounds and their effects.

Moreover, if ν_μ oscillates to ν_e and/or ν_τ, or even to a "sterile" neutrino, ν_s, (one with appreciably weaker interactions than the known neutrinos), comparison of the event rates

in each detector of ν_μ–, ν_e– and WNC(π^0)–induced reactions will permit the assignment of an observed decrease in the ν_μ event rate to a specific oscillation channel (or channels), and sharply delineate the values of Δm^2 and $\sin^2 2\theta$ in that channel. We repeat that the ratio of neutrino fluxes $\phi(\nu_e)/\phi(\nu_\mu)$ in a magnetic horn focused ν_μ beam at the AGS is approximately 10^{-2}, which will result in an appreciable increase in the $\nu_e n \to e^- p$ event rate if even a few percent of ν_μ oscillate to ν_e. And, observation of ν_μ disappearance without a proportional increase in the number of ν_e-induced events will be unambiguous evidence for oscillations in the $\nu_\mu \leftrightarrow \nu_\tau$ channel.

Taken together, these properties of the experimental arrangement provide tight control of possible systematic errors in the experiment—one of the foremost considerations in the design of the experiment—by monitoring the ν_μ and ν_e content of the beam at several locations along the beam path.

C. Far Detector Locations

The previous North Area neutrino beam at the AGS has been largely dismantled, and consequently a new beam must be designed and constructed. The direction of the beam is taken to be on a somewhat easterly line toward the north shore of Long Island. A detailed layout of a possible beam is shown in Fig. 2 in which the proton beam line is an extension of the present Fast Extracted Beam Line bent sufficiently to avoid RHIC and to direct it to the D24 and D68 detectors. Locations of the off-site detectors at Northville, L.I. (24 km) and on Plum Island (68 km) are shown in Fig. 3. At Northville, there is an extensive storage facility for gas and oil, consisting of tanks similar to those in this proposal. Space to locate the D24 detector is available to us and a provisional agreement has been authorized. There is a U.S. government facility on Plum Island, maintained by the Department of Agriculture and a provisional agreement to locate D68 there is in process. There is adequate water, electrical power, and security at these sites. It is fortunate that these sites are naturally located along the same line from the neutrino source, as described explicitly in Chapter V.

D. Detector Evolution

We expect the experiment to evolve in a continuous fashion, dictated by the rates at which construction and funding are likely to proceed. Our current plan involves the use of four identical detectors which permits operation as soon as each tank is completed, and facilitates the extraction of early physics results. We anticipate that the detectors will be built in the

sequence—D3, D24, D68, and the fourth detector most probably at D1. D3 and D24 could be complete by end of calendar 1998, and the additional tanks will be built in the succeeding year so that all 4 tanks would be in operation about one year later.

The first detector, located at D3, will permit early studies of the beam as soon as it is available, and detailed exploration of the detector performance. With the second detector (D24), significant searches for oscillations can begin. In one AGS run of 4 months, quasielastic event samples with statistical errors of approximately 0.3% and 2% (in D3 and D24, respectively) would be accumulated. As shown in Figure 4, most of the region allowed by the Kamiokande data could be excluded in this first run, or conversely, if the Kamiokande best fit value is correct, an effect of over 4 sigma in ν_μ disappearance would be observed. During this initial run we can also exclude the entire allowed region in Fig. I.3a for the appearance channel $\nu_\mu \to \nu_e$, as shown in Fig. 5; if the best fit value in that figure is correct, this initial run will yield a 10σ effect. The 4 month run the following year (run II) would include the tank at D68, and would either dramatically confirm the positive signal seen previously, then more than 5σ at D24, and 10σ at D68 in ν_μ disappearance at best fit, or extend the reach of the the experiment well below the allowed region in Fig. I.3b, as shown also in Fig. 4. In either case, the detector at D1 would provide high precision tests for possible systematic errors in our understanding of the detector performance, the neutrino beam behavior, and detector alignment. Finally, the ultimate reach of the experiment is shown in Fig. 4, which would be obtained from all 4 tanks and 16 months of running. The complete experiment would unequivocally solidify any result found earlier, and would extend the reach of the experiment below $3 \times 10^{-3} eV^2$ at $\sin^2\theta \simeq 1$, well below the lowest allowed value of Δm^2 in Figure I.3b. If an oscillation signal is found, the complete experiment will measure the oscillation parameters with an accuracy of 10 to 15% at the best fit point.

We continue this chapter with general descriptions of the neutrino beam and the detectors. In later sections we discuss the beam and detectors more fully, and event rates and backgrounds in the oscillation searches in detail.

E. Neutrino Beam

A useful figure of physics merit for an oscillation experiment is $\phi_\nu(E)\sigma_\nu(E)/E^2$, where $\phi_\nu(E)$ is the flux at a given detector, $\sigma_\nu(E)$ is the cross section for the dominant detected reaction, and $1/E^2$ arises in the oscillation probability for Δm^2 small. With $\phi_\nu(E)$ expressed as a flux $(\mathrm{GeV} - m^2 - \mathrm{POT})^{-1}$, L cancels out of the figure of merit. To optimize this product in a long

baseline experiment appears at first sight to be infeasible because the core of the neutrino beam produced by magnetic horn focusing of the secondary mesons (necessary for sufficient neutrino intensity) comprises higher energy neutrinos than are present at larger radii; and it is the core of the beam which is usually planned to be seen by distant detectors. It is, nevertheless, possible to reach an approximate optimization in a long baseline experiment such as E889, as will be demonstrated below. First, however, it is useful to show that detailed measurements of a neutrino beam at the AGS with incident proton energy of 28 GeV agreed well with earlier calculations of the properties of that beam, indicating the approximate 10% level of confidence that may be placed in neutrino beam calculations.

Shown in Fig. 6 are the measured and calculated ν_μ fluxes produced by 28 GeV protons at the AGS [1], with magnetic horn focusing of the secondary mesons. This beam, which was measured at a distance of 100 m from its source (proton target), has been studied in detail, as have the neutrino interactions induced by it. Note the agreement between the calculated and measured spectra, and also that between the calculated and measured ratios $\phi(\bar{\nu}_\mu)/\phi(\nu_\mu)$ and $\phi(\nu_e)/\phi(\nu_\mu)$, specifying the opposite helicity and ν_e contaminations in the ν_μ beam, which are shown in Figs. 7 and 8, respectively. The calculated and measured radial dependence are shown in Fig. 9.

It is particularly interesting to note the properties of the quasielastic reaction which are determined from those beams, and are shown in Fig. 10. The plot of proton energy deposited in the vertex cell (Fig. 10b) is well reproduced by calculation, and conveys the dominance of low Q^2 transitions in quasielastic scattering. Here $Q^2 \approx 2M_pT_p$ where T_p is the proton kinetic energy.

The E-889 collaboration has produced a ν–beam simulation based on the programs GEANT 3.21 + FLUKA (hadronic package) in which proton secondary interactions within the proton target are calculated and there is no modification of particle production cross sections. A test of this work, done at TRIUMF, is shown in Fig. 11 which compares the result of the TRIUMF Monte Carlo calculation with data shown earlier in Fig. 6. We have utilized this beam simulation package in the experimental design described in what follows.

The neutrino fluxes at various distances from the proton target have been calculated for $E_p = 28$ GeV with the program above. Fig. 12 compares the flux at a short distance shown in Fig. 6 with that expected at 1 km and 3 km, all on the center line of the beam. The appreciable increase in average energy of the beam at 1 km relative to that at the shorter distance is clearly evident, and is an issue of first importance in the design of a long baseline neutrino oscillation experiment. By 1 km, however, the flux dependence on increasing distance

is approximately $1/r^2$, and further energy hardening of the beam irradiating an 18 m diameter $\times$ 18 m high detector is small, approximately 1–2% in average energy, as shown by the flux at 3 km.

In the experimental design for E889, the radial dependence of the energy of the neutrinos in the beam, indicated in Fig. 9, provides the means of circumventing the energy hardening of the beam at the long baseline distances. We simply offset the detectors from the central line of the beam by a fixed angle, which is possible because the longitudinal distances involved are relatively so large. We show in Fig. 13 the neutrino fluxes at D1, D3, D24, and D68 as they would be if the detectors were to be located on the beam center line or at an angle of 1.5 degrees with respect to that line. It is clear that the beam shape at 1.5 degrees is to a good approximation identical in all four detectors, unlike the differing shapes in the detectors on the center line of the beam. Furthermore, the off-center line flux is increased in absolute value at low energy and depleted at higher energies relative to the zero degree flux, two additional significant advantages. Finally, the variation in beam intensity with respect to the midline of D1 is 33% across the entire diameter of D1. For D3, the variation is less than 10% relative to the midline, and negligible for D24 and D68. See Fig. III A.9. This variation does not cause any systematic difficulties as shown in Chapter V because the variation is to a good approximation linear across the detectors. Furthermore, the total variation in intensity over the small central region of D1 through which pass the neutrinos reaching D24 and D68 is less than 4%, which will be determined with precision by measurement over the entire fiducial volume of D1, still another advantage and not, as commonly conjectured, a disadvantage. This technique of off-setting the detectors allows the experiment to be run at a high incident proton energy and correspondingly high neutrino intensity, while keeping the average neutrino energy low. It is discussed in detail in Section III A.

F. The Detectors

The Cherenkov technique is well understood and well tested over long time periods. A detector—Kamiokande II—similar in essentials to those proposed here is shown in Fig. 13 to help fix ideas. The proposed E889 detector is shown in Fig. 1 of III B. The imaging Cherenkov counter has the property of providing good angular and energy resolution as well as particle identification of ν_μ– and ν_e–produced muons and electrons which are contained within the detector. To illustrate this feature, we show in Figs. 15 and 16 the actual event data [2] for a muon and an electron, respectively, and Monte Carlo simulations of those events

for comparison. Note the sharpness of the outer edge of the Cherenkov ring of the muon as compared to that of the electron, and the increased amount of large angle radiation produced by the electron. These characteristics among others are the bases for algorithms used by the Kamiokande and IMB collaborations to identify successfully muons and electrons and separate them one from the other. WNC (π^0) events are efficiently ($\sim 75\%$) identified (see Chap. IV. below), which in most instances can be shown to be consistent with the π^0 mass.

In this connection, it is of interest to note the results of tests made by the Kamiokande group with a 1 kiloton imaging water Cherenkov detector at KEK. Muons and electrons of several known different momenta were injected at several different positions into the 10 m high $\times$ 10 m diameter detector. The resulting rings were analyzed using the same algorithms employed in identification of the atmospheric neutrino events. The data from the 1 kiloton test detector confirm the high efficiency of particle identification claimed in the analysis of the atmospheric neutrino events. See Chapter IV.

The choice of the Cherenkov technique is dictated by the requirements of a large mass to serve as combined target-detector for the neutrino interactions, unrestricted visibility within the detector, and relatively low cost for such large mass. Provision of a 4π solid angle, highly efficient veto counter within the detector tank is straightforwardly accomplished. The same technique will be employed in the future detectors for the Sudbury Neutrino Observatory and Superkamiokande, whose extensive design studies and cost estimates have contributed significantly to the design of the experiment proposed here.

Each detector tank is 18m in diameter filled with water to a depth of 18m. Above the water level a catwalk for access and support is provided (see Fig 13 of Sec III B). Each tank will be equipped with an array of about 2550 photomultipliers (PMT), each 20cm in diameter. 2200 of these PMT are placed on the inner surface of a 15m high by 15m diameter cylinder, while the remainder view the outer annular volume 1.5m thick which functions as a veto to discriminate against cosmic rays and to tag tracks leaving the fiducial volume. The inner PMT array must be able to locate the trajectory of single particles accurately in time and space, to measure the total energy deposited, and to identify neutrino events having single muons, electrons, pizeros, or multiparticle final states. The PMT array covers 6.5% of the area of the inner cylinder, and this is enhanced by Winston cones to over 10.4%. More details of the detector and its implementation are given in Sec III B.

Much of the system design has been replicated from similar detectors under construction in Japan and Canada. The electronics chain from SNO is well suited to the needs of this experiment. The major differences in application arise from the operation of the detectors

on the earth's surface which necessitates dealing with the 80KHz rate of cosmic rays, and the need to synchronize timing data at widely separated sites with the neutrino beam from the AGS. The former poses no additional problems since the SNO electronics has been designed to handle bursts from supernovae that are in excess of the combined beam and cosmic rates for the closest detector. The latter requires development of a sophisticated timing system that is described in detail in Sec III C.

There are several reasons why the four detectors in E889 are identical. These have to do with the control of systematic errors which are likely to constitute the limiting factor in any long baseline neutrino oscillation experiment, and indeed may be the cause of a spurious result.

(i) Neutrino beams are different from other particle beams in that they are especially dependent at the 10-20% level of uncertainty on the detailed behavior of the focusing system. Consequently, precise knowledge of a given neutrino beam cannot be obtained from Monte Carlo simulations, but requires measurement in an adequate neutrino detector. A comparable uncertainty is present in the simulation of the detector response, which compounds the difficulty. If it is required that there be minimal or no dependence of the experimental result on Monte Carlo simulation of the beam properties or detector response, it is necessary to have two identical detectors, separated in space by a moderate distance and aligned, to measure both the beam properties and the detector response separately and precisely. This is particularly important in achieving a sufficiently precise quantitative understanding of the beam for the offset detectors in E889, and for detectors of such large dimensions as in E889.

(ii) Once having determined the detector properties with high statistics in the two upstream detectors, D1 and D3, it is vital to have detectors of identical mass and construction, i.e., identical response, at the far sites to be able to utilize directly the knowledge of the event selection criteria, the fiducial volume constraints, the event containment criteria, and possible detector limitations from the upstream detectors. No Monte Carlo based predictions of event rates or event or detector properties are necessary for identical detectors in contrast to the simulations required in making extrapolations from smaller upstream to larger downstream detectors or from detectors of one type to detectors of another type. With the arrangement of the four detectors along the same line (see Chapter V), this experiment with identical detectors becomes essentially a simple counting experiment.

(iii) The raw cosmic ray event rates in the four detectors are high since the detectors are at ground level. It is straightforward to minimize the effect of those rates on the experiment by a 4π solid angle anticounter surrounding each inner detector, which provides both active

and passive shielding, and by making use of the time structure of the fast extracted proton beam of the AGS. These are discussed in detail in Chapter V. Another advantage of making all the detectors identical is that the effort to eliminate background and dead time due to the cosmic ray flux is the same for all the detectors and no individual detector corrections which might limit sensitivity to oscillations are necessary.

(iv). As far as cost saving is concerned, it is easy to show that no significant saving is achieved by a modest reduction in size of D1 and D3, while an appreciable reduction in size would defeat the purpose outlined in (i) and (ii) above. Alternatively, an increase in size of D24 and D68 quickly runs up their cost disproportionately beyond the cost of increased beam time to achieve the same statistical precision in those detectors. At a cost of approximately \$1.5M per kiloton for the completed detectors of E889, they are a bargain when their capabilities are considered.

G. Event Rates

There are three event types that constitute the signals of E889: WCC types $\nu_\mu n \to \mu^- p$ and $\nu_e n \to e^- p$, and the WNC type $\nu N \to \nu N' \pi^0$. All others comprise the backgrounds. At the low neutrino energies involved, ν_τ interact only in the WNC mode. The complete analysis of signals and backgrounds is in Chapter V. We summarize some of the results here.

The cross section $\sigma(\nu_\mu n \to \mu^- p)$ has been measured [3] as a function of E_ν as has $d\sigma(\nu_\mu n \to \mu^- p)/dQ^2$ [1]. The single pion production neutrino cross sections have been calculated with reasonable accuracy, and also studied experimentally in both bubble chambers and electronic detectors. Extensive references to both theory and experiment are given in [4]. We use this cross section material as input to our Monte Carlo calculation which includes the detailed neutrino beam and detector properties to obtain the results given here.

In calculating the event rates we assume a fiducial volume of 1725 m^3 per tank (6.5 m radius and 13 m height), and a total of 8.8×10^{20} POT or 16 months of running at 4×10^{13} POT per AGS pulse with 20 hr days. We note that these assumption are quite conservative. The actual volume of the detector tank including the veto volume will be a factor of 2.65 larger, and the AGS has exceeded 6×10^{13} POT per pulse.

$\underline{\nu_\mu n \to \mu^- p}$

The integral $\int \sigma(E)\phi(E)dE$ over the interval $0 < E_\nu < 5$ GeV is 1.66×10^{-47} at D1 when the measured quasielastic cross section including the effects of Pauli suppression in

	D1	D3	D24	D68
Contained $QE(\mu)$	5.21×10^6	5.80×10^5	9102	1136
Deficit with $\Delta m^2 = 0.01$ eV^2				
$\sin^2(2\theta) = 1.0$	–	–	1214	694
Reconstructed $NC(\pi^0)$	10.2×10^5	11.3×10^4	1773	221
$QE(e)$ Beam and π^0 bkgd.	1.63×10^5	1.81×10^4	284	35
Excess with $\Delta m^2 = 0.01$ eV^2				
$\sin^2(2\theta) = 1.0$	–	–	1008	706

Table 1: *Expected reconstructed $QE(\mu)$, $QE(e)$, and $NC(\pi^0)$ events in the detectors of E889 after 8.8×10^{20} POT or 16 months of running. The expected deficit of muons and excess of electrons in the far detectors with $\Delta m^2 = 0.01$ eV^2 and full mixing is also shown.*

light nuclei is used. There are 2.68×10^{23} neutrons per gm of water. Therefore the number of events in D1 will be 4.43×10^{-15}/kTon/POT. From simulations using the neutrino spectrum, 0.77 of the μ^- from $\nu_\mu n \to \mu^- p$ produced in the fiducial volume will be contained, i.e., stop in the visible volume of a detector tank (15 m diameter by 15 m height) and yield a clear Cherenkov ring. The product of all these factors gives the number of contained quasielastic events in D1. The rates in D3, D24, and D68 to can be calculated to good accuracy by using $1/r^2$ scaling. The actual nature of this scaling and the systematic error are discussed in Chapter V. These quasielastic event rates are shown in Table 1. The expected deficit in case of oscillations with the Kamioka best fit parameters is also shown. There will be additional background reduction cuts on the momentum and the direction of the muon that will be analysis specific; these will not impact the rates shown in Table 1 significantly.

Since the quasielastic events account for about 0.60 of the total cross section at these energies, there will be more than 300 events per month of all types in D68, more than 2400 per month in D24 and much more in the near detectors, so that adequate evaluation of the progress of the experiment will be available.

$\underline{\nu n \to \nu n \pi^0 \text{ and } \nu p \to \nu p \pi^0}$

The weak neutral current reactions with a single final state π^0 (WNC (π^0)) are known to be produced at approximately 20% of the total quasielastic rate [4] in the neutrino beam of

Fig. 17. Momentum distributions of the final state π^0 from each of the WNC (π^0) reactions are shown in Fig. 18. The mean momentum of the π^0s ($\sim$ 300 MeV/c) is such that for most pions the two decay photons are well separated in angle and thereby produce two clear showering Cherenkov rings. By several independent eyescans we have determined that the π^0s can be identified with an efficiency of 54% (see Chapter IV) if we require two complete rings and 75% if we require 1 complete ring and extra energy [5]. Accordingly, the WNC (π^0) rates in the four E889 detectors are approximately (0.2×0.75) times the total $QE(\mu^-)$ rates. These are shown in Table 1.

The detection of WNC (π^0) events at the above rates allows for normalization of the quasielastic μ^- rate in each detector by means of the ratio WCC (QE μ^-)/ WNC (π^0), since the WNC (π^0) reactions are independent of the flavor of the incident neutrino. In the absence of neutrino oscillations, that ratio should be constant in all four detectors. For completeness, we note that in the unlikely case of oscillations to a sterile neutrino, $\nu_\mu \leftrightarrow \nu_s$ a decrease in the WNC (π^0) rate will accompany a decrease in the QE (μ^-) rate by the same fractional change.

$\underline{\nu_e n \rightarrow e^- p}$

At neutrino energies above 200 MeV, the cross sections for the quasielastic reactions induced by ν_μ and ν_e are approximately equal. We have calculated that the ν_e contamination in our magnetic horn focused ν_μ beam at 1.5 degrees will be 10^{-2}. The e^- in the $e^- p$ final state have a lower threshold momentum than μ^- for Cherenkov radiation, and the e^- containment is essentially unity. The electrons will be recognized as single ring events with a characteristic showering ring pattern without a clean edge. The methods for recognizing showering rings are well understood and we expect to have essentially no background from muon to electron misidentification above 400 MeV. The most significant background to electron rings will be from neutral current produced π^0s with one of the decay photons missing or the two rings from the two photons overlapping. We have performed a detailed calculation of this background in Chapter V. Including the π^0 background, in the absence of neutrino oscillations, $(\nu_\mu \rightarrow \nu_e)$ showering single ring events will appear in each detector at a rate of about 4% relative to the total μ^- from $\nu_\mu n \rightarrow \mu^- p$. Table 1 shows the number of single ring showering events above a cut of 500 photoelectrons along with the expected excess in the case of oscillations. If neutrino oscillations occur in the channel $\nu_\mu \rightarrow \nu_e$ at the level of even a few percent, the fractional increase in the observed number of e^- from $\nu_e n \rightarrow e^- p$ will be very large and

clearly identify that oscillation channel.

In summary, the three signal event types in E889 occur with rates that allow for consistency checks and normalization internal to each detector as well as by comparison of rates among the detectors. This statistically significant control of the systematic errors is, in our opinion, the *sine qua non* of any neutrino oscillation experiment that seeks to measure with precision a real effect as opposed to setting another limit. Finally, the three signal event types will unambiguously determine the neutrino oscillation channel in most of the explored parameter space.

H. Conclusions of Section II

In this chapter, the assumptions behind the design and the general nature of the proposed experiment have been discussed. Emphasis has been given to the strategy of carrying out the experiment in evolutionary fashion which will yield results at the earliest time, consistent with expected rates of funding and detector construction. Brief descriptions of the experimental arrangement and the promise of each step were given, and also of the neutrino-induced event types and their rates from which redundant signals of neutrino oscillations may be extracted. In a period as short as 4 months beginning early in 1999, we expect to acquire 2275 contained quasielastic muon events and 71 quasielastic electron events in D24, to search for ν_μ-disappearance and ν_e appearance at the levels indicated by the contours in Figs. 4 and 5. In later data-taking with three or all four detectors in place, we will reach the boundaries shown in Figs. 4 and 5. Finally, by measurements of muons, electrons, and neutral pions, we expect to specify the oscillation channel, $\nu_\mu \rightarrow \nu_e$, $\nu_\mu \leftrightarrow \nu_\tau$, or both, unambiguously.

References

1. L.A. Ahrens, Phys. Rev. D34, 75 (1986); ibid 35, 785 (1987).

2. E.D. Frank, Ph.D. Thesis, University of Pennsylvania, 1992 (unpublished).

3. S.J. Barish et al., Phys. Rev. D16, 3103 (1977).

4. M. Nakahata et al., Jour. Phys. Soc. Japan 55, 3786 (1986).

5. For Kamioka this efficiency factor has been studied by T. Kajita. T. Kajita, in Workshop on Atmospheric Neutrinos, Louisiana State University, Baton Rouge, LA, May, 1993 (unpublished).

Figure Captions

Figure 1. Schematic representation of the long baseline neutrino oscillation experiment proposed here.

Figure 2. Tentative schematic layout of the proposed neutrino facility.

Figure 3. (a) Direction of the proposed neutrino beam and location of the Northville and Plum Island sites. (b) Detail of the Northville site. (c) Detail of the Plum Island site.

Figure 4. Exclusion plot of Δm^2 vs $\sin^2 2\theta$ for $\nu_\mu \to \nu_x$ to be reached in 4, 8 and 16 months of data-taking with two, three, and four detectors as described in the text.

Figure 5. Exclusion plot of $\Delta m^2\theta$ vs $\sin^2 2\theta$ for $\nu_\mu \to \nu_e$ to be reached in 4, 8, and 16 months of data-taking with two, three, and the full complement of 4 detectors.

Figure 6. The ν_μ flux calculated and measured at the AGS ($E_p = 28.3$ GeV). The flux from 28.3 GeV protons obtained in a scintillator-wire chamber experiment (E734) at the AGS [13] with magnetic horn focusing, a decay length of 57 m, a 20 m long shield, and another 23 m to the detector is $1.3 \times 10^{-3}\nu_\mu$ per (m^2 - GeV - POT) at the peak of the curve.

Figure 7. Measured and calculated ratio $\phi(\bar{\nu})/\phi(\nu_\mu)$ corresponding to the flux in Fig. 6.

Figure 8. Measured and calculated ratio of $\phi(\nu_e)/\phi(\nu_\mu)$ corresponding to the flux in Fig. 6.

Figure 9. Measured and calculated radial dependence of the ν_μ flux in Fig. 6 in different intervals of E_ν.

Figure 10. Measured and calculated properties of $\nu_\mu n \to \mu^- p$; (a) θ_μ-distribution, and (b) energy deposited in vertex cell vs E, both from [2].

Figure 11. Monte Carlo simulation of the ν_μ flux in Fig. 6 by the beam program described in the text. This program is used in all beam calculations below.

Figure 12. Comparison of calculated ν_μ fluxes at 1 km and 3 km with that measured at 100 m from the target. All on beam axis.

Figure 13. Comparison of spectra for D1, D3, D24, and D68 located on axis (0^0) and 1.5^0 off axis.

Figure 14. Kamiokande detector.

Figure 15. Observed Cherenkov ring from a muon in the Kamiokande II detector. The lower displays are simulated for an electron (left) and muon (right) with the same vertex position, direction, and momentum as the observed event. Solid curves are rings reconstructed from timing and pulse height measurement in each PMT.

Figure 16. Same as Fig. 15 but for an observed electron event. Simulations correspond to the observed event.

Figure 17. Comparison of the neutrino beam shape produced by 12.4 GeV protons (ANL, ZGS) and the beam shape at 1.5^0 off axis produced by 28.3 GeV protons at 1 km from the source.

Figure 18. (a) Momentum spectra of π^0 from $\nu_\mu n \to \mu^- p\pi^0$ and WNC final states $\nu n\pi^0$ and $\nu p\pi^0$ (b) Spectra of ν_μ producing π^0 in (a).

Figure 19. Comparison of atmospheric ν_μ spectrum with AGS 28.3 GeV produced spectrum at 1.5^0 off axis.

BROOKHAVEN NATIONAL LABORATORY
AGS Expt 889

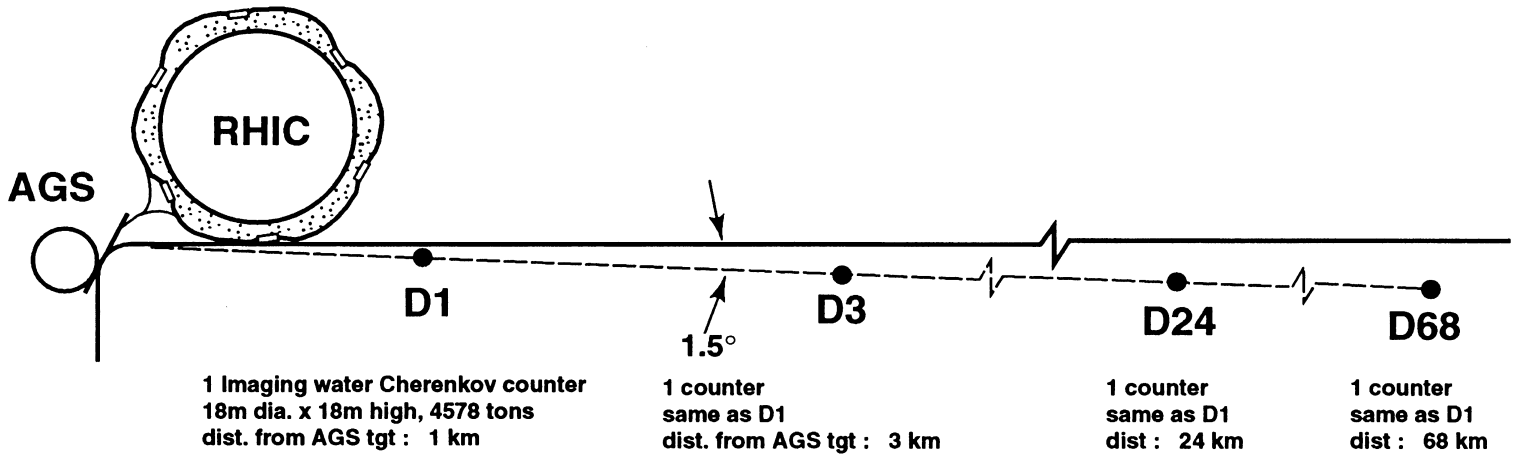

Fig. 1

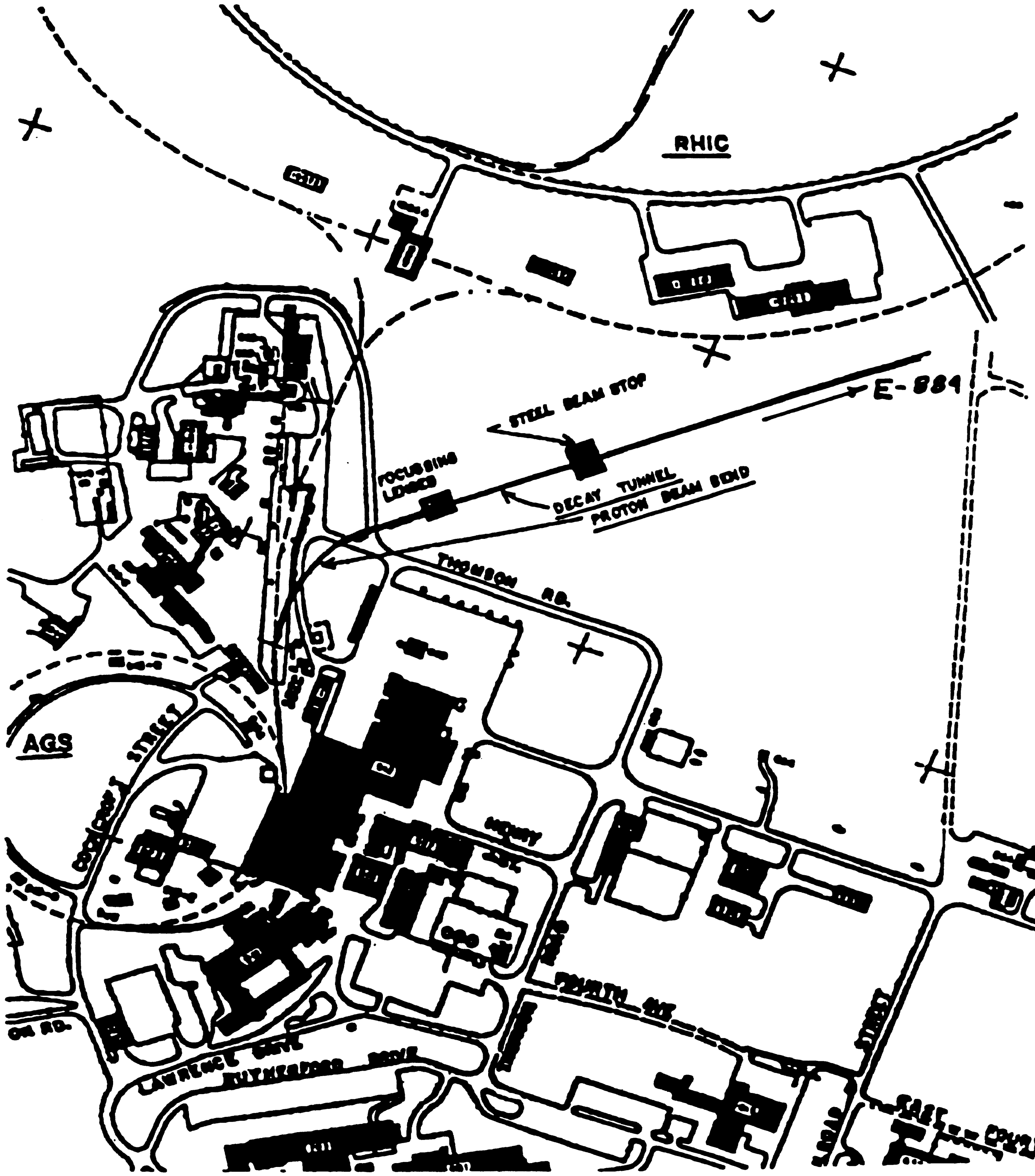
RHIC
E-881
STEEL BEAM STOP
FOCUSSING LENSES
DECAY TUNNEL
PROTON BEAM BEND
THOMSON RD.
AGS
FOURTH AVE
STREET

Fig. 2

Map of Long Island

Fig. 3a

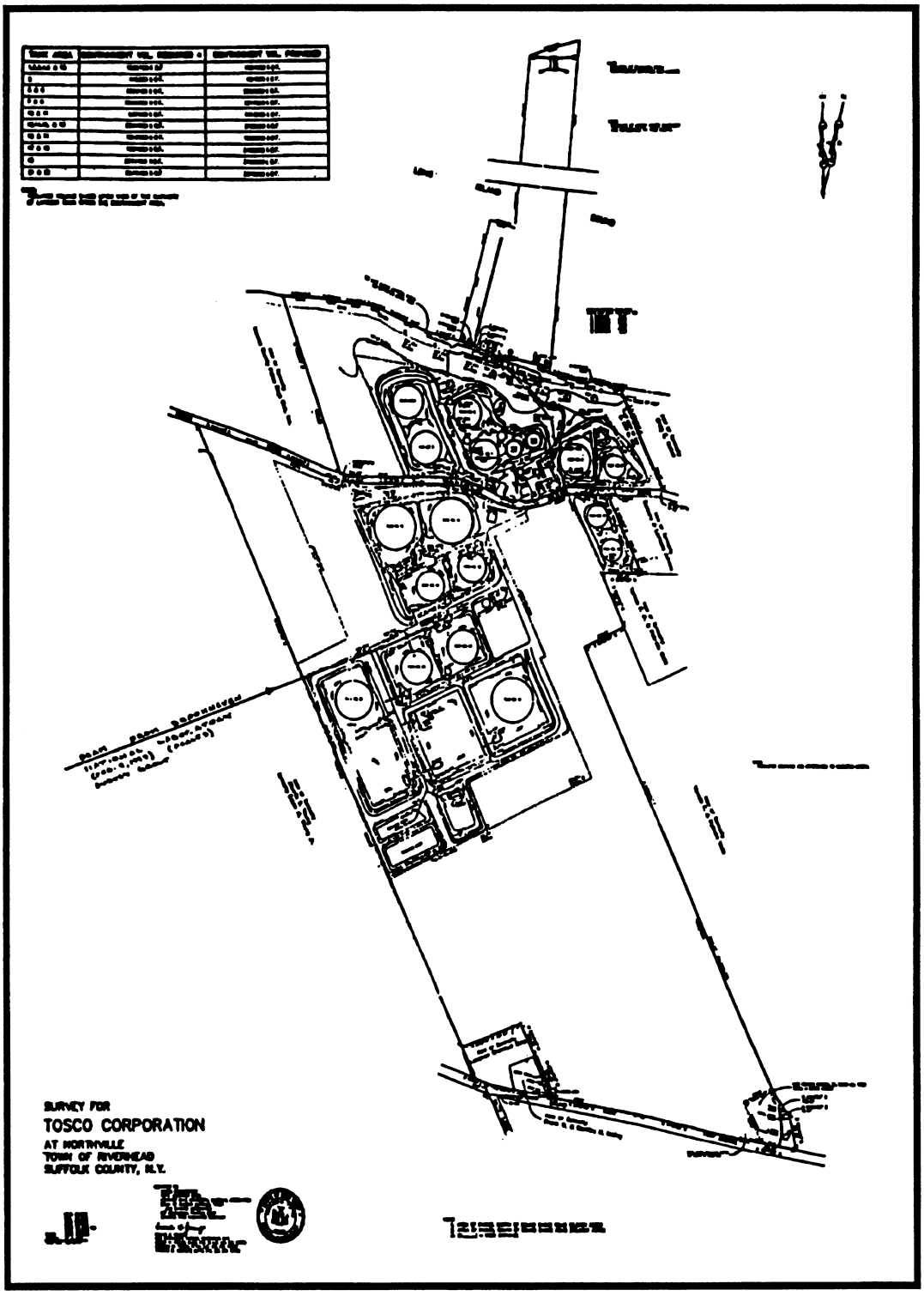
SURVEY FOR
TOSCO CORPORATION
AT NORTHVILLE
TOWN OF RIVERHEAD
SUFFOLK COUNTY, N.Y.

Fig. 3b

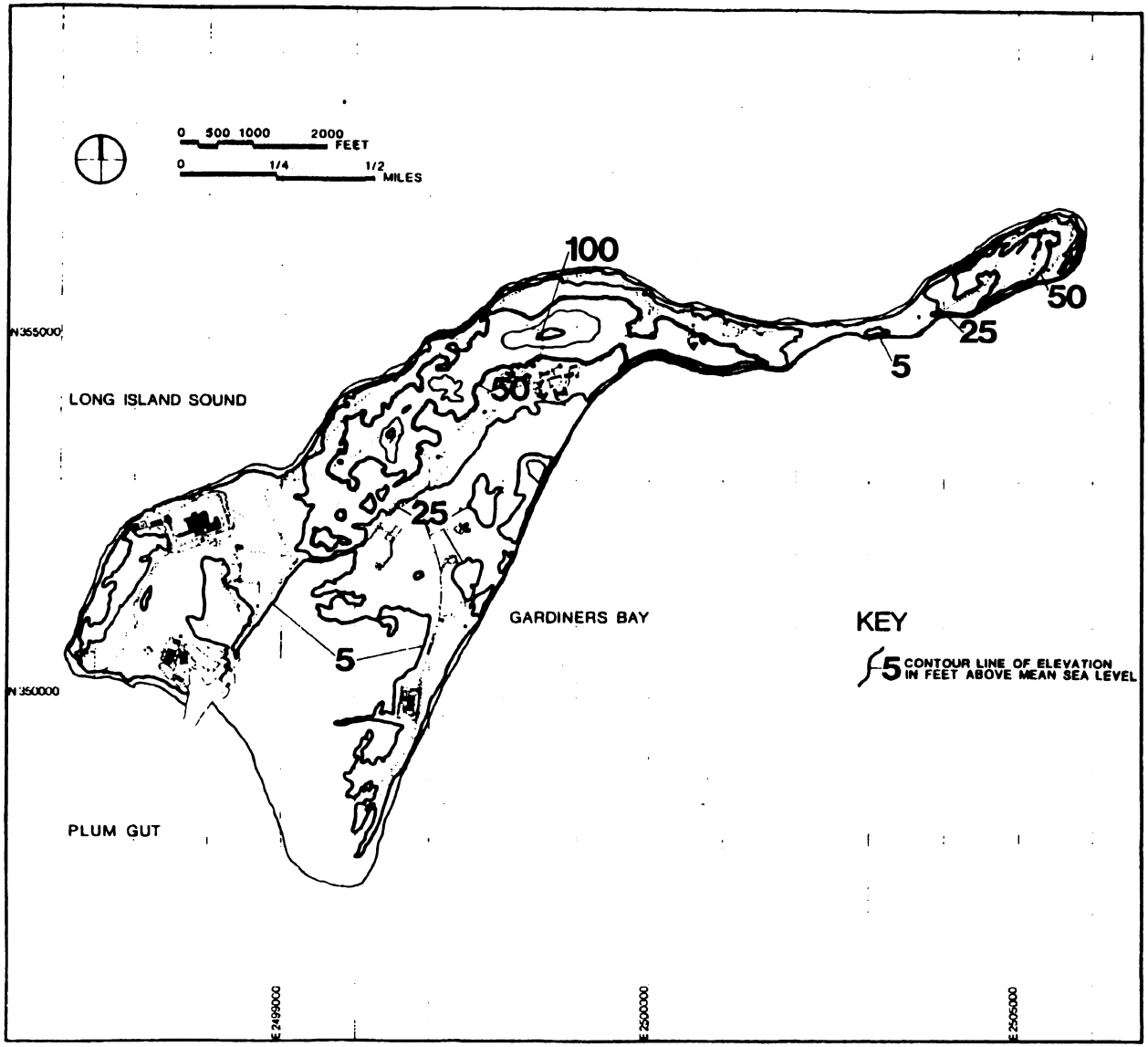

PLUM ISLAND ANIMAL DISEASE CENTER

GREENPORT, L.I., N.Y.

MASTER PLAN

January 24, 1977

Topography

Perkins & Will Architects

Perkins & Will/Architects
445 Hamilton Avenue, White Plains, N.Y.

Dubin-Bloome/Consulting Engineers
42 West 39th Street, New York, N.Y.

B3

Fig. 3c

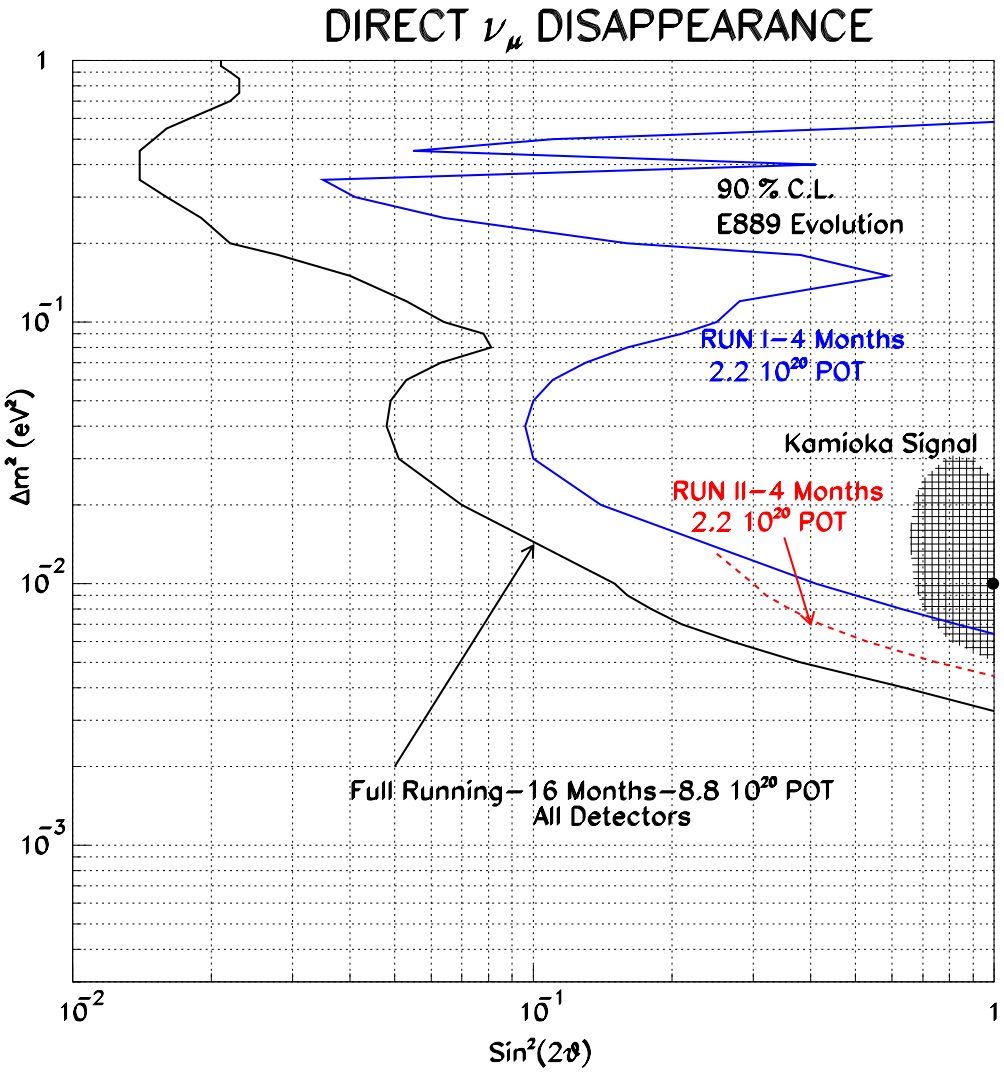
DIRECT ν_μ DISAPPEARANCE
90 % C.L.
E889 Evolution
RUN I–4 Months
2.2 10^{20} POT
Kamioka Signal
RUN II–4 Months
2.2 10^{20} POT
Full Running–16 Months–8.8 10^{20} POT
All Detectors
Δm^2 (eV^2)
$\sin^2(2\vartheta)$
1
10^{-1}
10^{-2}
10^{-3}
10^{-2}
10^{-1}
1

Fig. 4

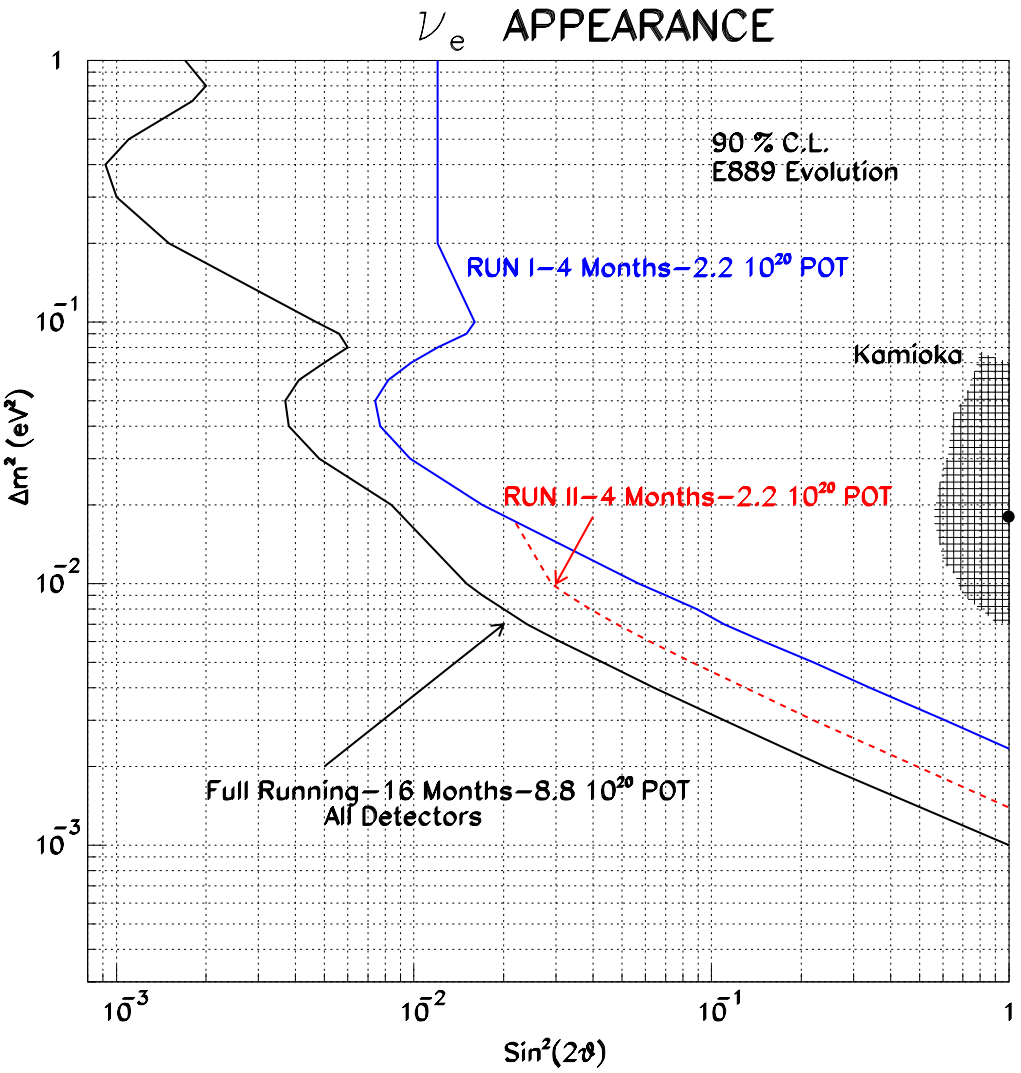
ν_e APPEARANCE
90 % C.L.
E889 Evolution
RUN I–4 Months–2.2 10^{20} POT
Kamioka
RUN II–4 Months–2.2 10^{20} POT
Full Running–16 Months–8.8 10^{20} POT
All Detectors
Δm^2 (eV^2)
Sin^2(2θ)
1
10^{-1}
10^{-2}
10^{-3}

Fig. 5

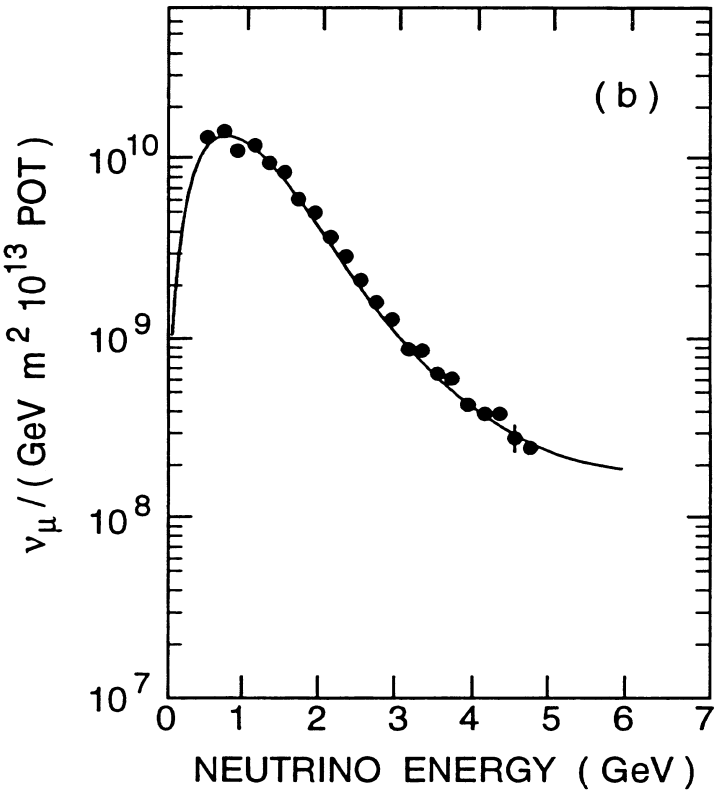
(b)
10^{10}
10^{9}
10^{8}
10^{7}
ν_μ / (GeV m^2 10^{13} POT)
0
1
2
3
4
5
6
7
NEUTRINO ENERGY (GeV)

Fig. 6

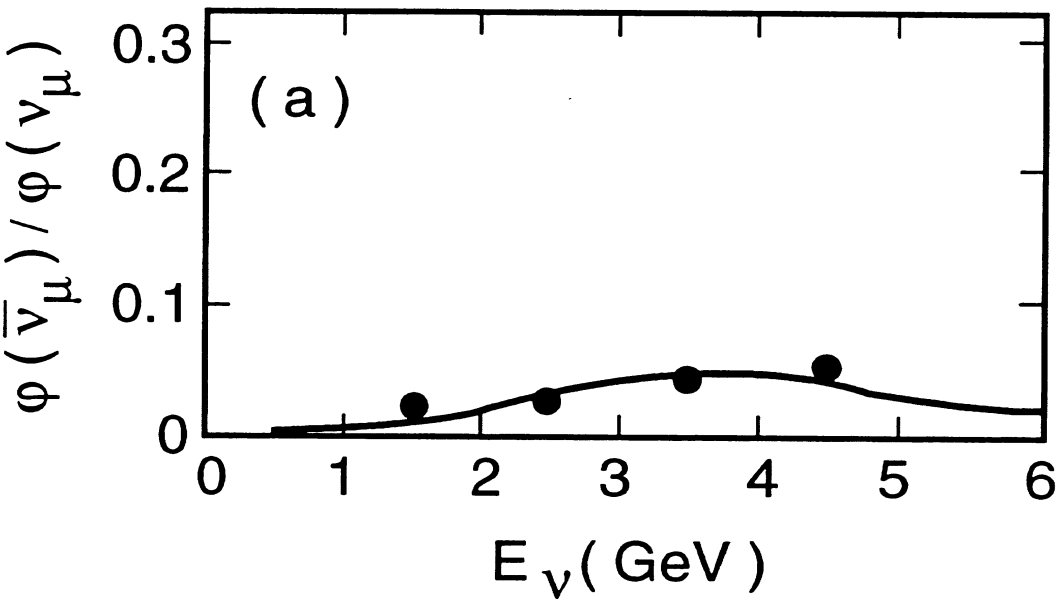

Fig. 7

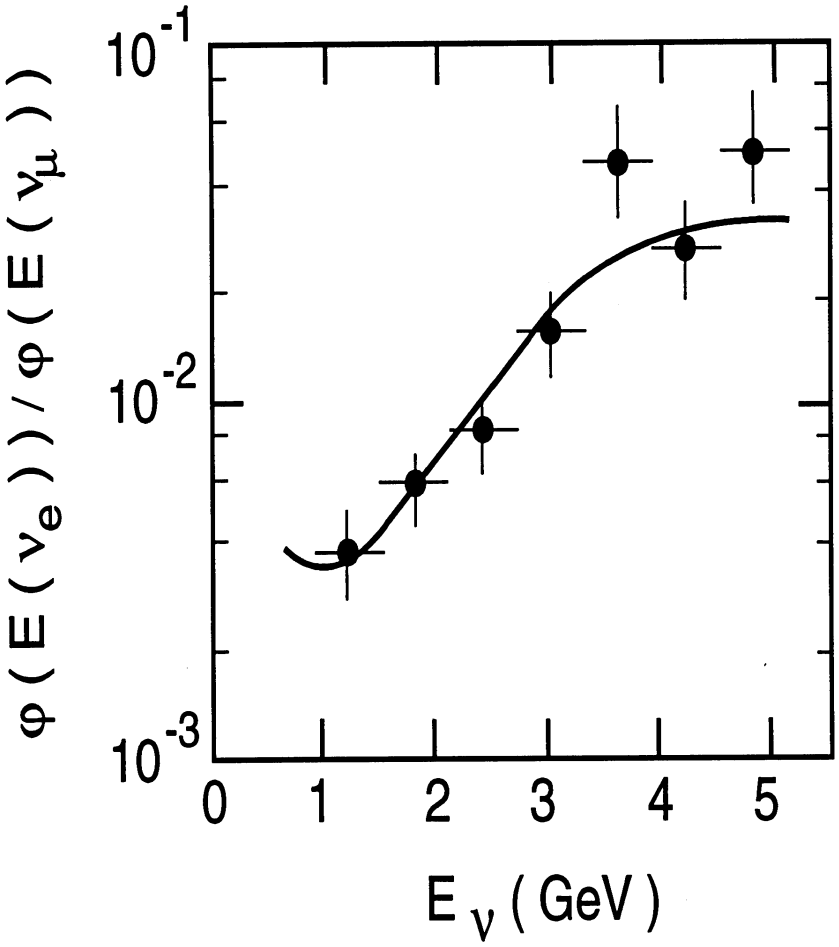

Fig. 8

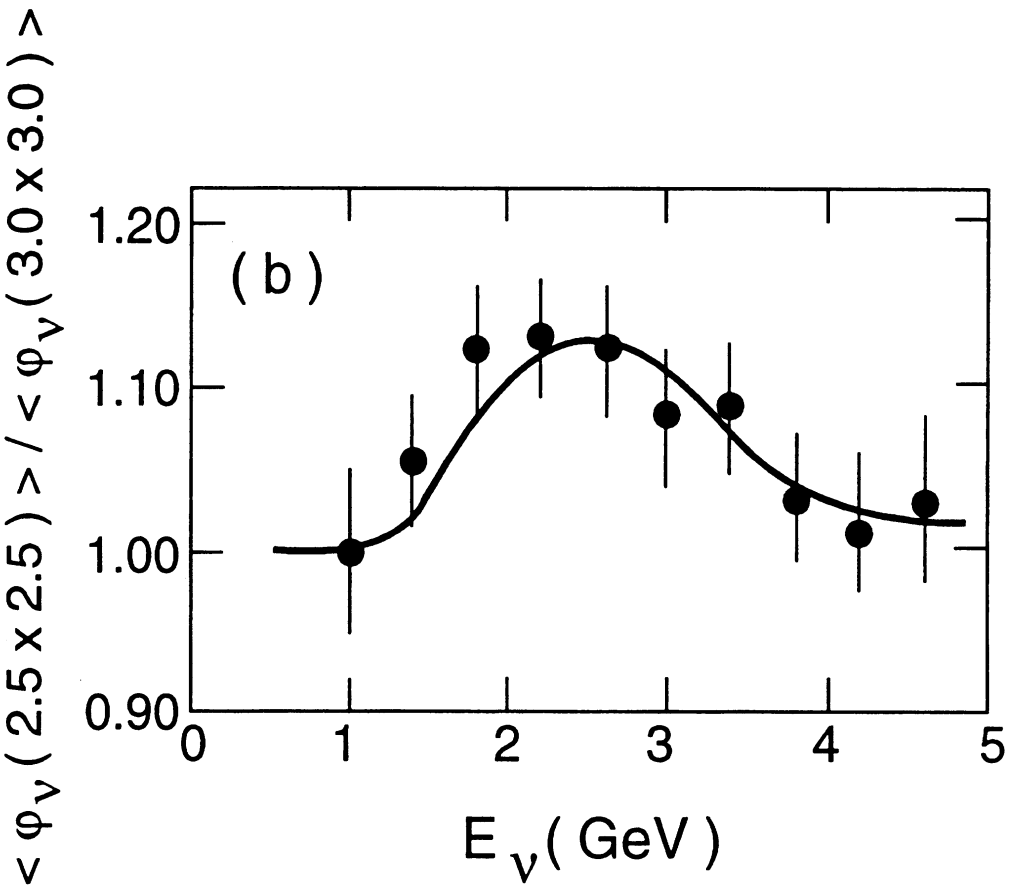
(b)
1.20
1.10
1.00
0.90
0
1
2
3
4
5
E_ν(GeV)
$< \varphi_\nu (2.5 \times 2.5) > / < \varphi_\nu (3.0 \times 3.0) >$

Fig. 9

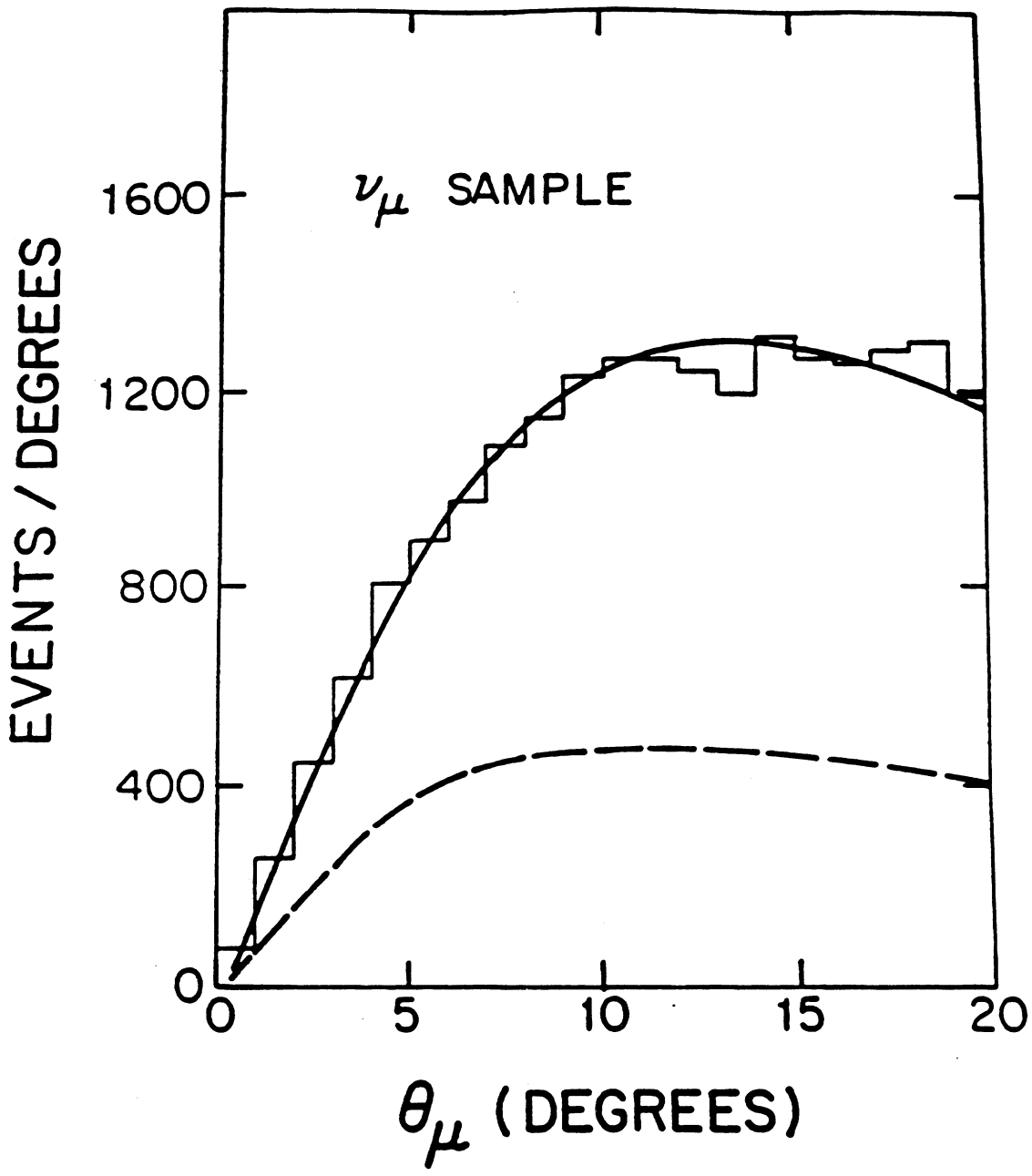
ν_μ SAMPLE
EVENTS / DEGREES
1600
1200
800
400
0
0
5
10
15
20
θ_μ (DEGREES)

Fig. 10a

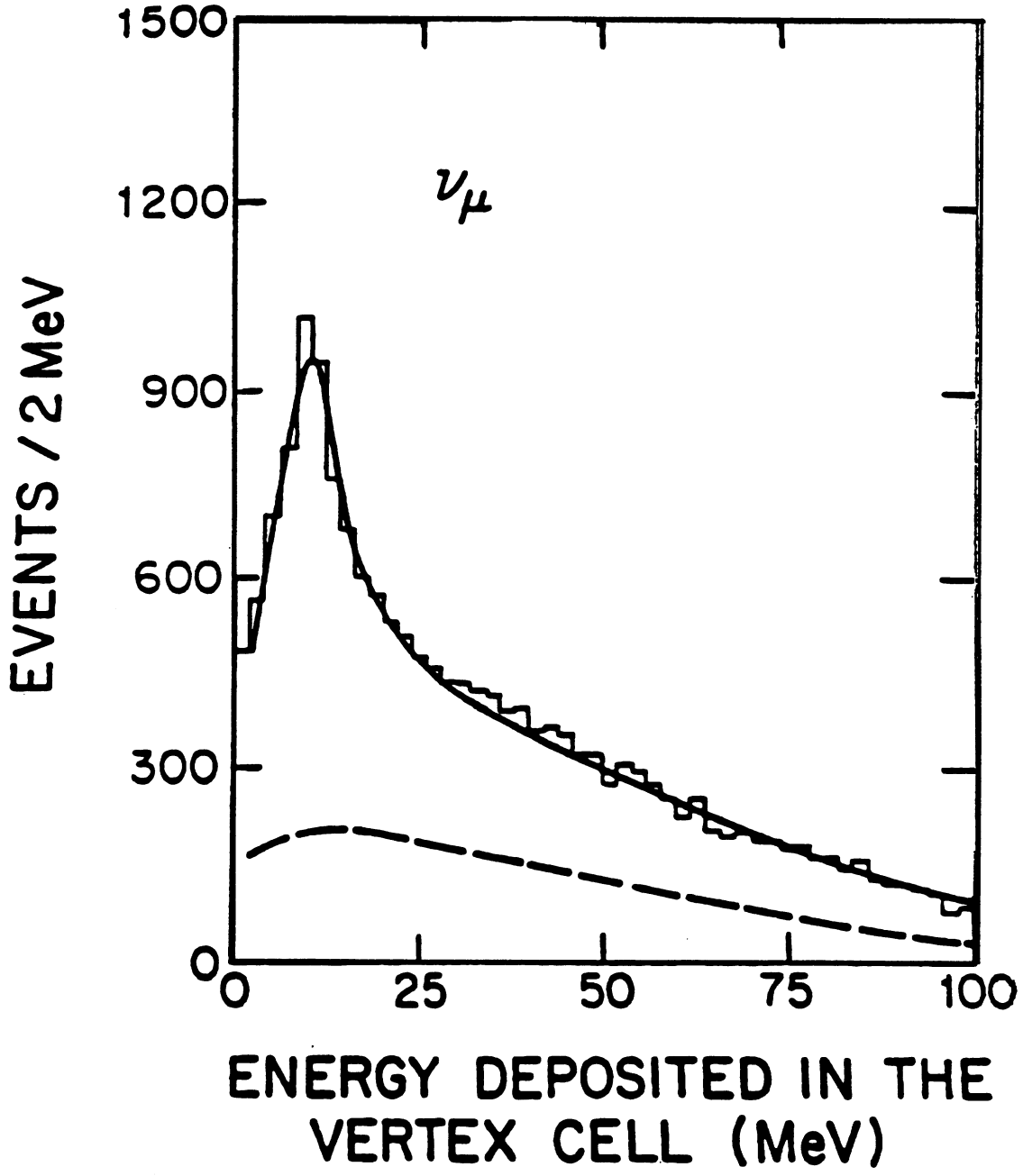
1500
1200
900
600
300
0
ν_μ
EVENTS / 2 MeV
0
25
50
75
100
ENERGY DEPOSITED IN THE
VERTEX CELL (MeV)

Fig. 10b

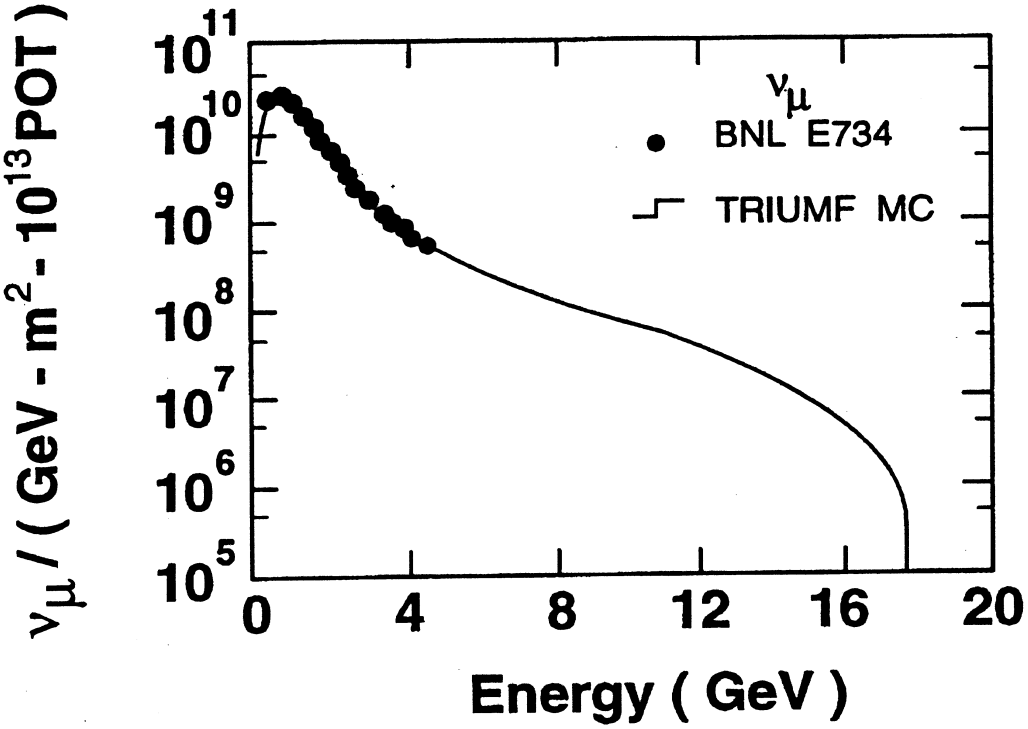
ν_μ / (GeV - m^2 - 10^{13}POT)
10^{11}
10^{10}
10^9
10^8
10^7
10^6
10^5
0
4
8
12
16
20
Energy (GeV)
ν_μ
BNL E734
TRIUMF MC

Fig. 11

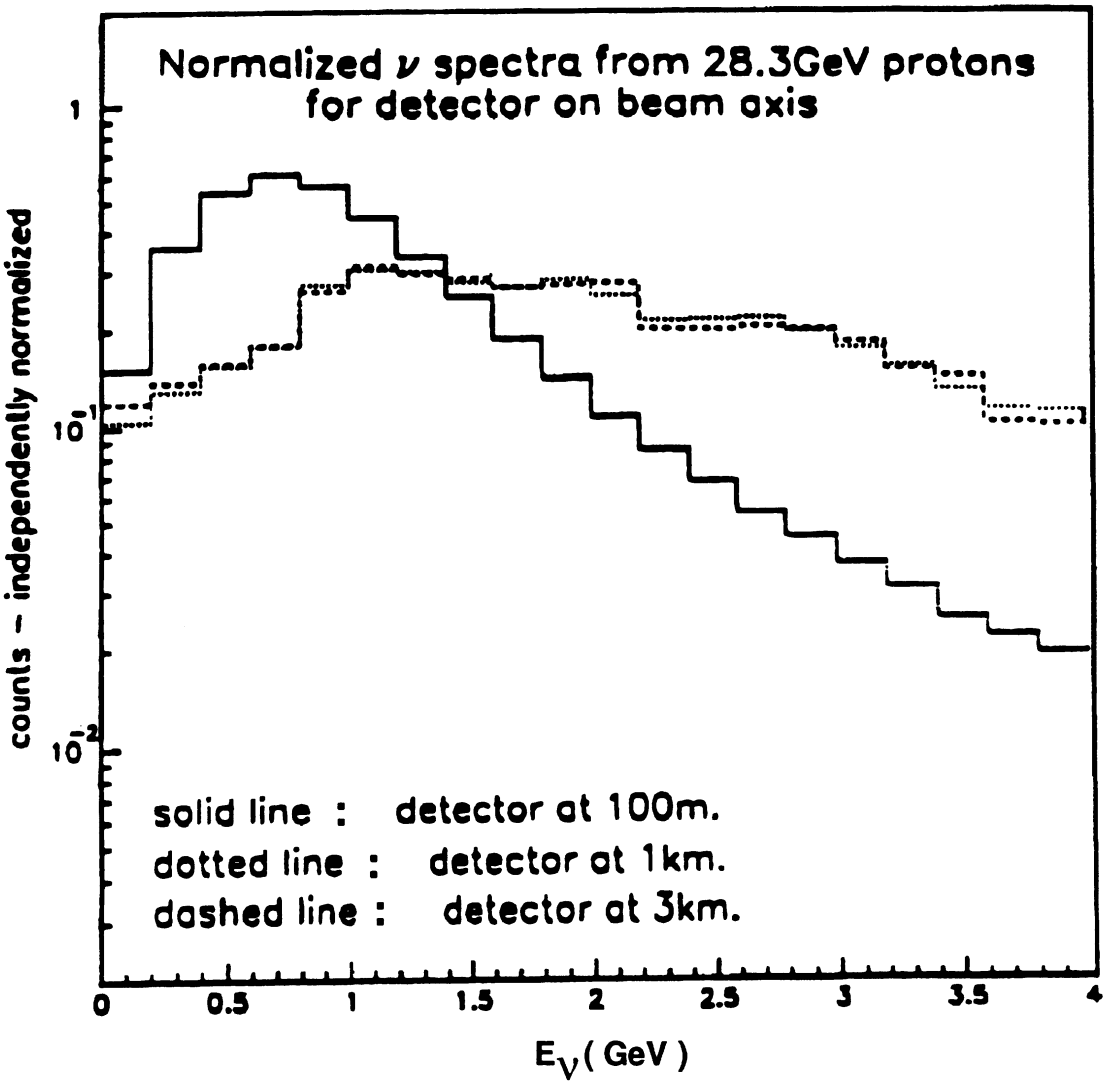
Normalized ν spectra from 28.3GeV protons
for detector on beam axis
counts - independently normalized
1
10^{-1}
10^{-2}
solid line : detector at 100m.
dotted line : detector at 1km.
dashed line : detector at 3km.
0
0.5
1
1.5
2
2.5
3
3.5
4
E_ν (GeV)

Fig. 12

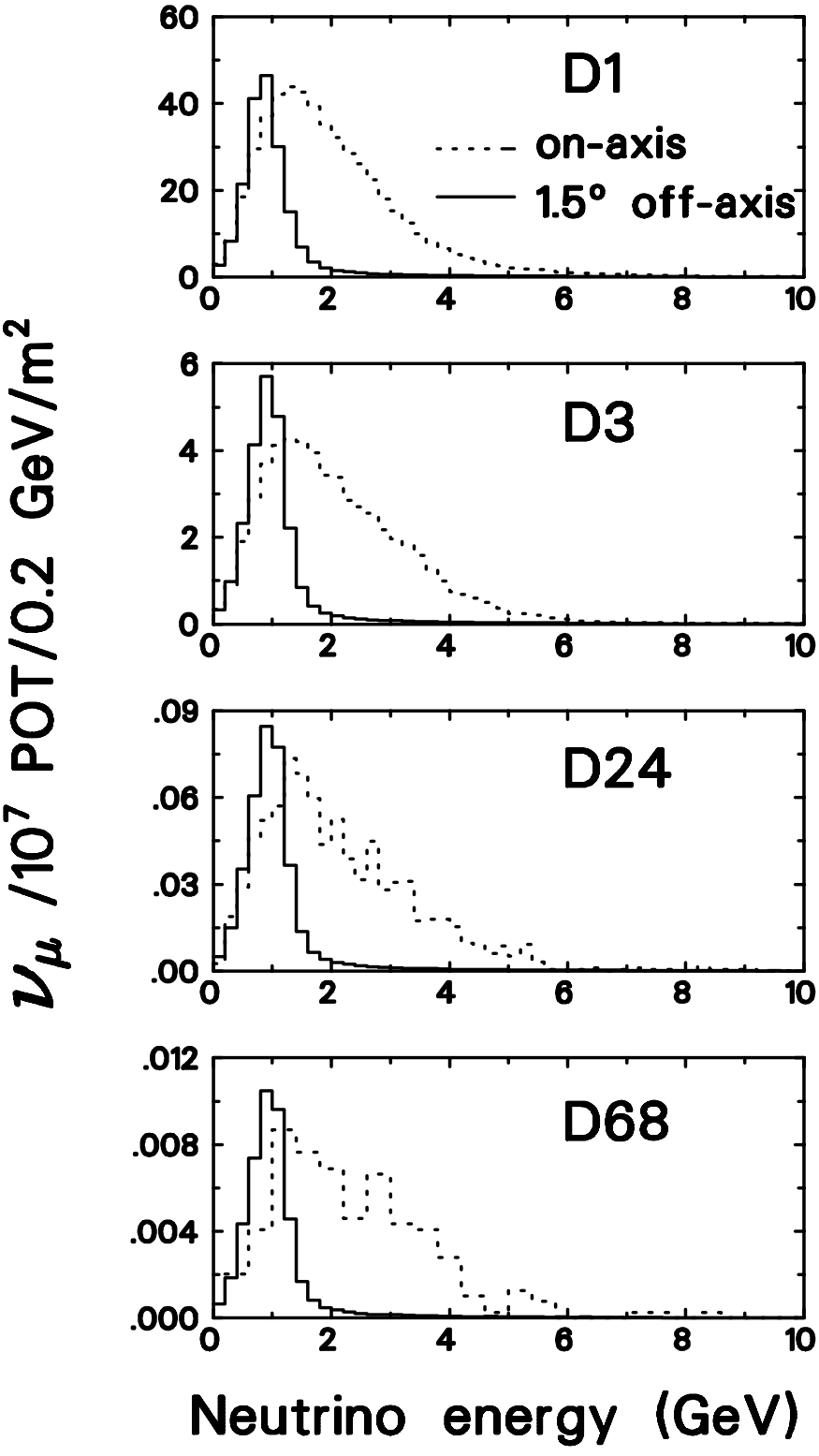
D1
on-axis
1.5° off-axis
D3
D24
D68
ν_μ /10^7 POT/0.2 GeV/m^2
Neutrino energy (GeV)

Fig. 13

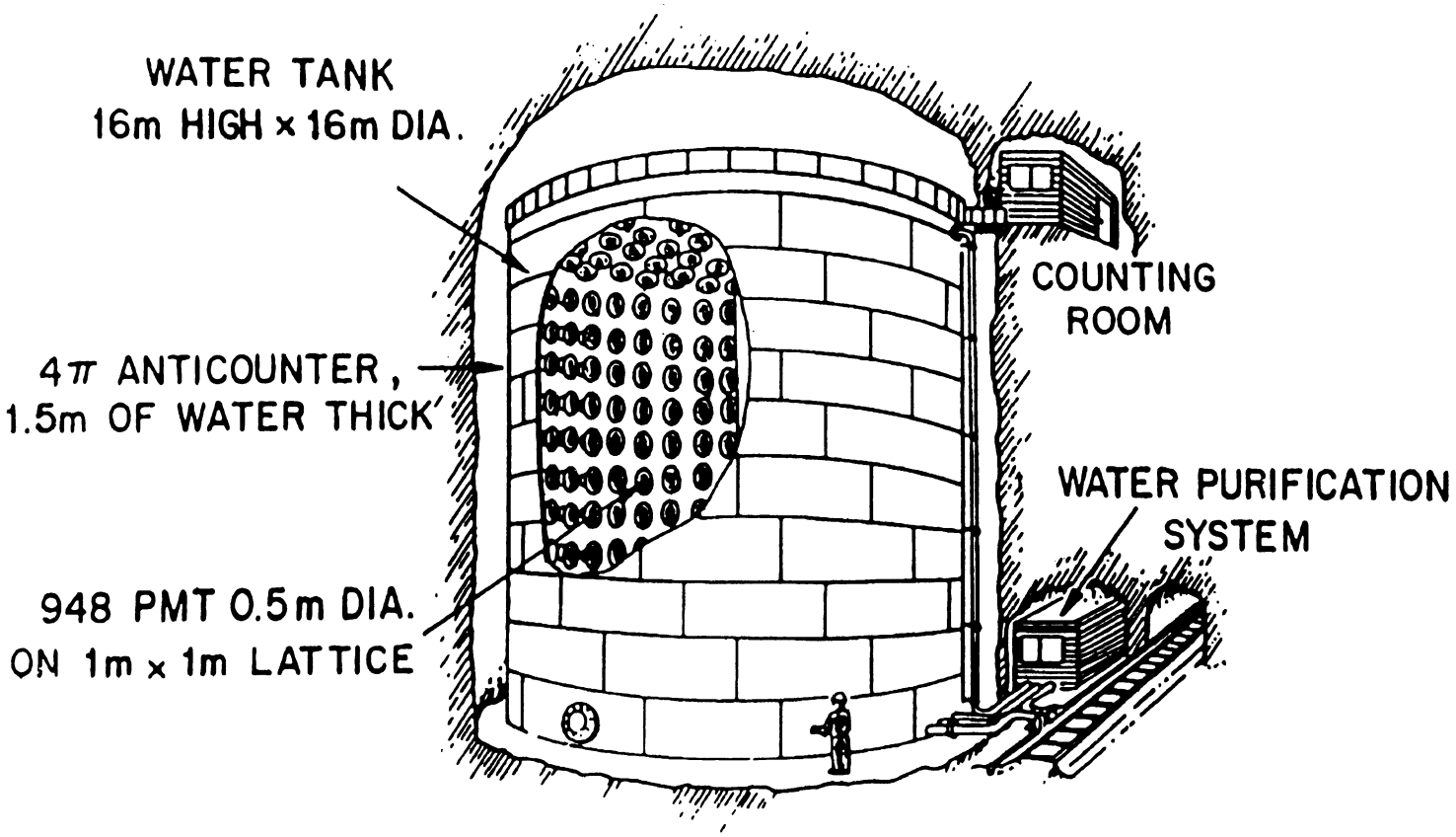
WATER TANK
16m HIGH × 16m DIA.
4π ANTICOUNTER,
1.5m OF WATER THICK
948 PMT 0.5m DIA.
ON 1m × 1m LATTICE
COUNTING
ROOM
WATER PURIFICATION
SYSTEM

Fig. 14

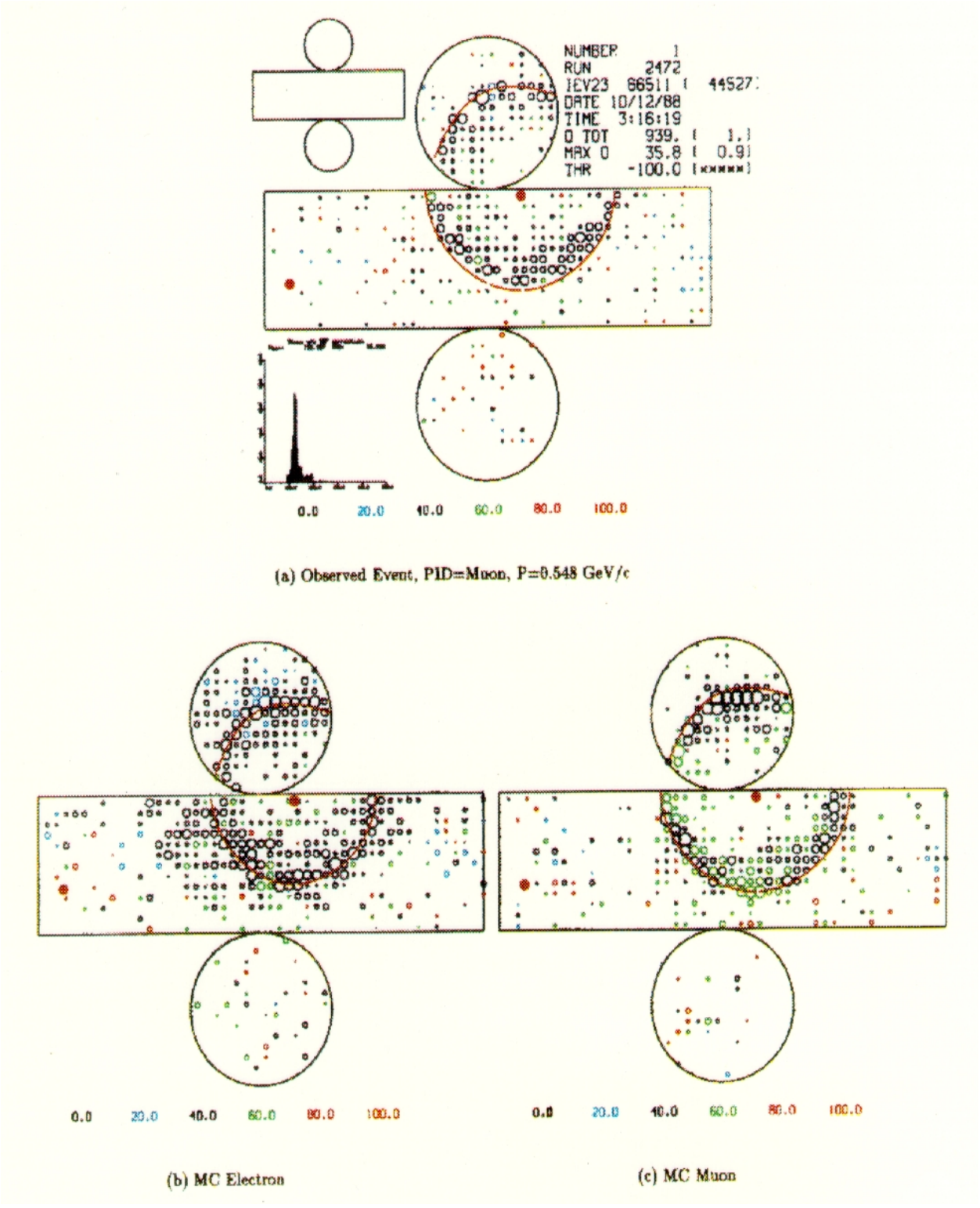

(a) Observed Event, PID=Muon, P=0.548 GeV/c

(b) MC Electron

(c) MC Muon

Fig. 15

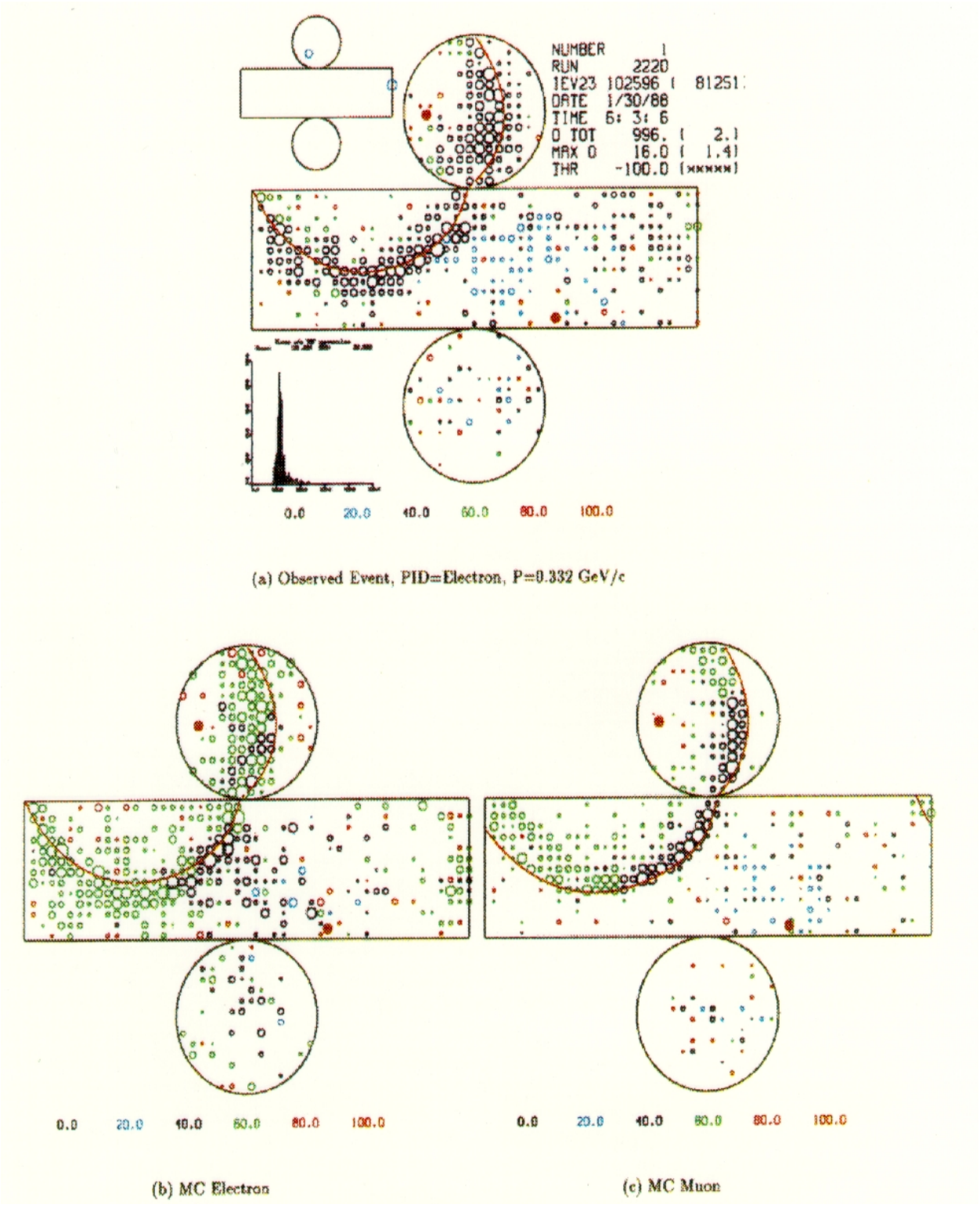

(a) Observed Event, PID=Electron, P=0.332 GeV/c

(b) MC Electron

(c) MC Muon

Fig. 16

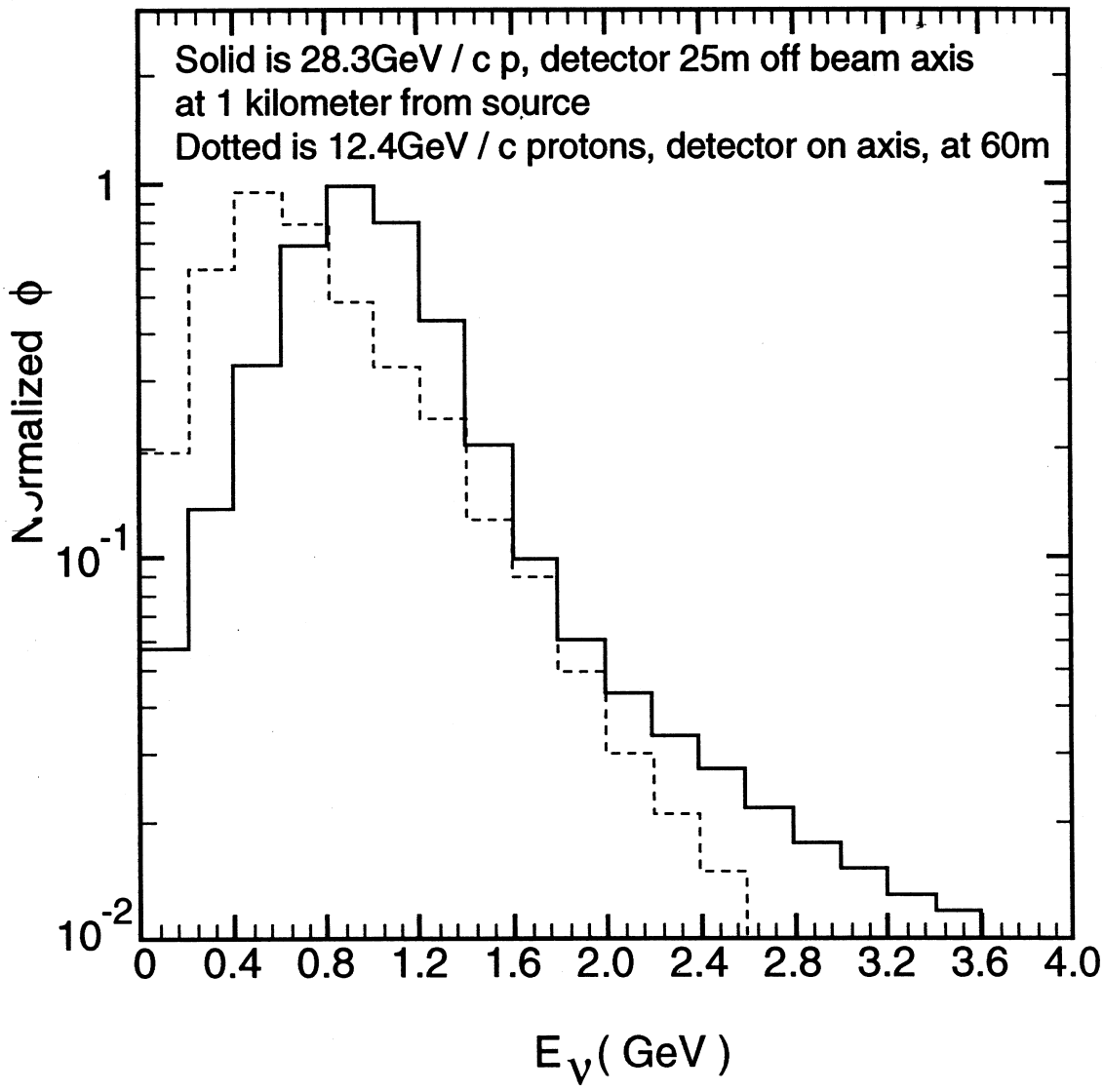
Solid is 28.3GeV / c p, detector 25m off beam axis
at 1 kilometer from source
Dotted is 12.4GeV / c protons, detector on axis, at 60m
Normalized φ
1
10^-1
10^-2
0
0.4
0.8
1.2
1.6
2.0
2.4
2.8
3.2
3.6
4.0
E_ν (GeV)

Fig. 17

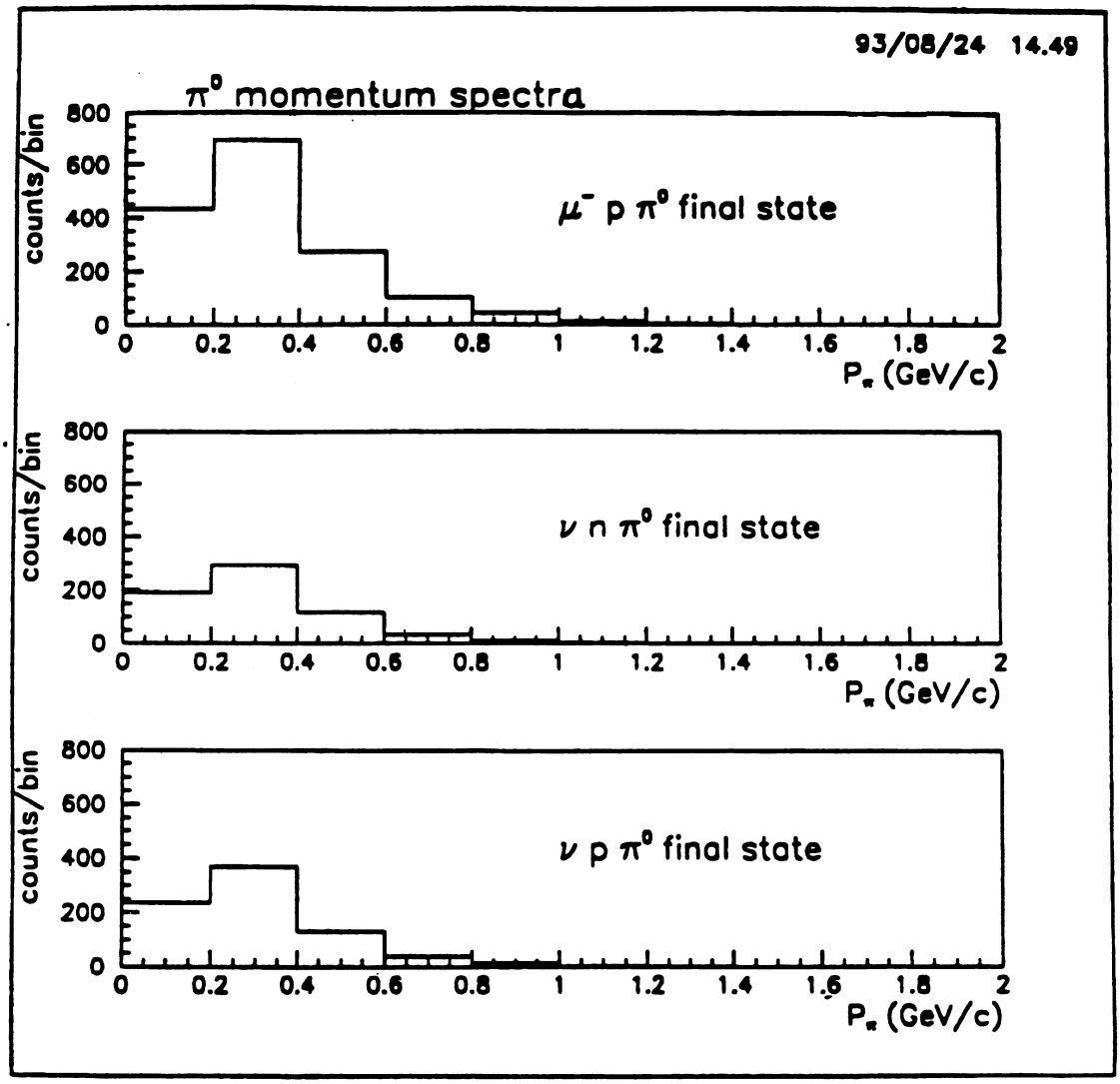
93/08/24 14.49
π⁰ momentum spectra
counts/bin
μ⁻ p π⁰ final state
ν n π⁰ final state
ν p π⁰ final state
P_π (GeV/c)

Fig. 18a

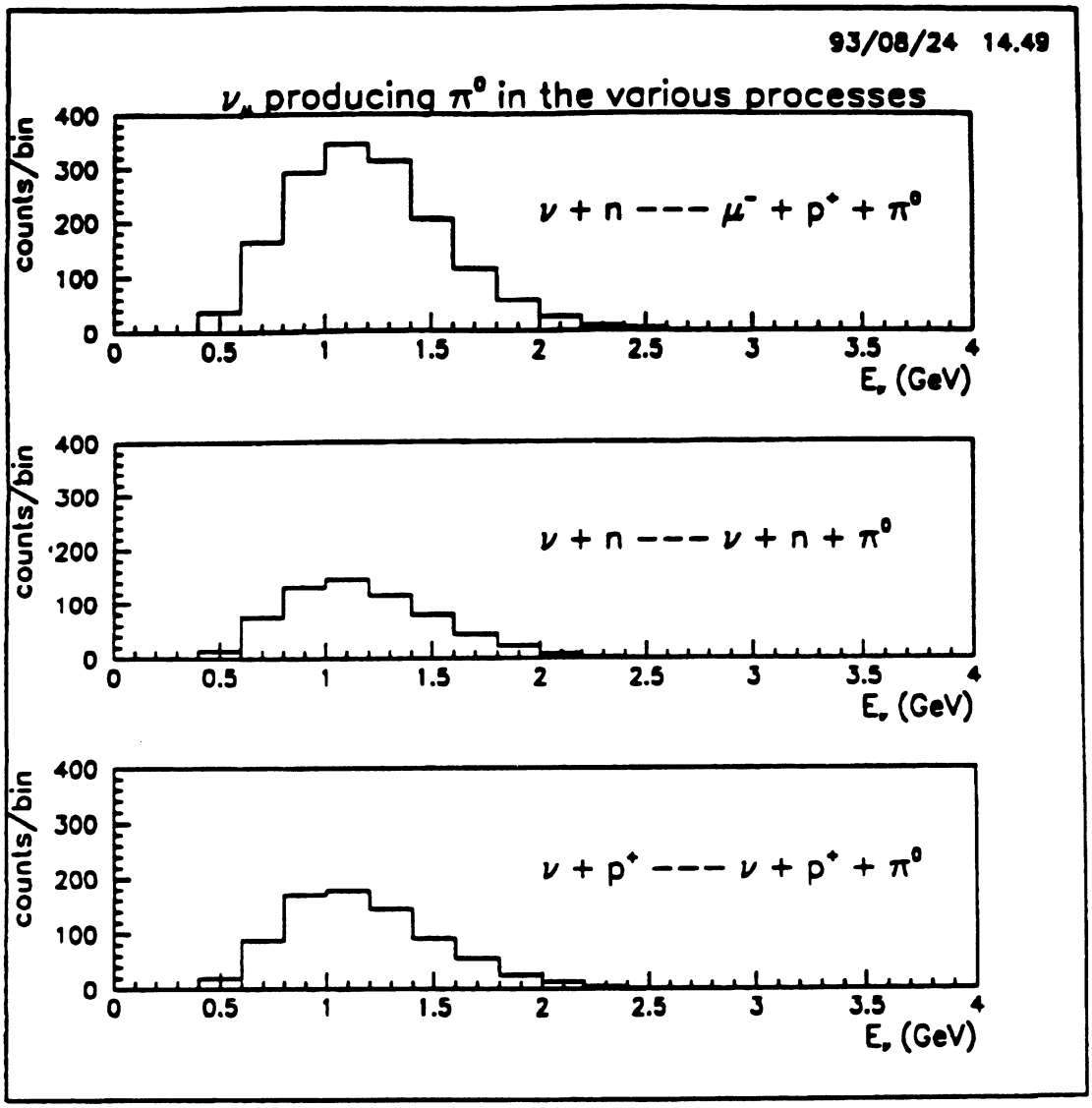
93/08/24 14.49
ν_μ producing π^0 in the various processes
counts/bin
400
300
200
100
0
0
0.5
1
1.5
2
2.5
3
3.5
4
E_ν (GeV)
$\nu + n \text{ --- } \mu^- + p^+ + \pi^0$
$\nu + n \text{ --- } \nu + n + \pi^0$
$\nu + p^+ \text{ --- } \nu + p^+ + \pi^0$

Fig. 18b

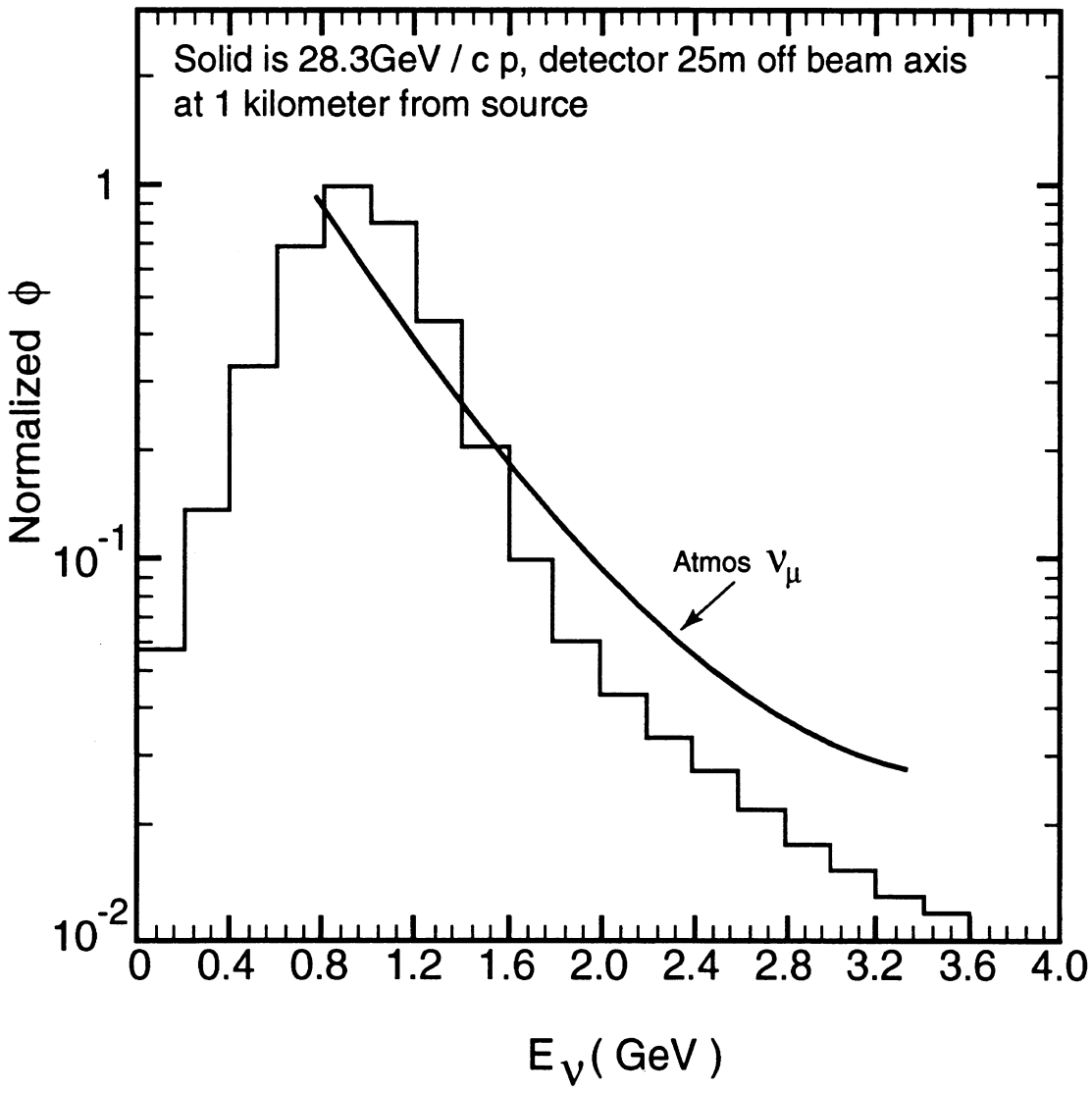
Solid is 28.3GeV / c p, detector 25m off beam axis
at 1 kilometer from source
Normalized ϕ
1
10^-1
10^-2
Atmos ν_μ
0
0.4
0.8
1.2
1.6
2.0
2.4
2.8
3.2
3.6
4.0
E_ν (GeV)

Fig. 19